**A NEW IMAGE PROCESSING ALGORITHM FOR COMPUTER AIDED**

**PREDICTION OF GLAUCOMA IN GHANA**

By

Prince Ebenezer Adjei

BSc. Biomedical Engineering (Hons)

A Thesis submitted to the Department of Computer Engineering, Kwame Nkrumah University of

Science and Technology in partial fulfillment of the requirements for the degree of

Master of Philosophy

Department of Computer Engineering

College of Engineering

MAY 2016

# DECLARATION

I hereby declare that this submission, to the best of my knowledge, contains no material previously published nor material which has been accepted for the award of a degree by this or any other University, except where due acknowledgment has been given in the text.

_____                                    _____
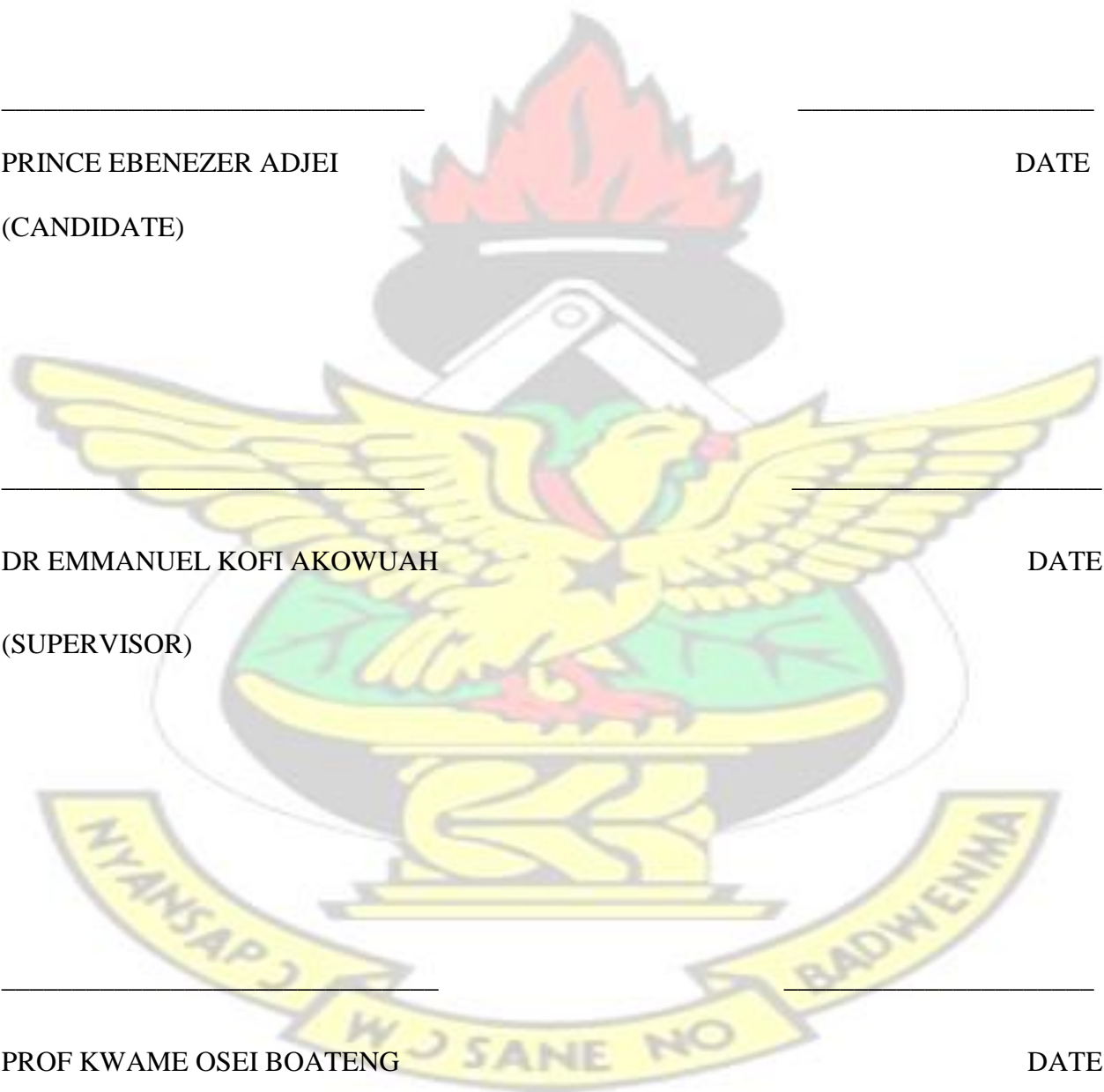
PRINCE EBENEZER ADJEI                                                          DATE

(CANDIDATE)

_____                                    _____

DR EMMANUEL KOFI AKOWUAH                                              DATE

(SUPERVISOR)

_____                                    _____

PROF KWAME OSEI BOATENG                                               DATE

(HEAD OF DEPARTMENT)

# KNUST

## ABSTRACT

Glaucoma is a term that describes a family of eye diseases that damage the optic nerve. About 8% of the entire population of Ghanaians above the age of 30 suffer from what is known as Primary Open Angle Glaucoma (POAG). The nemesis of POAG is blindness. POAG usually presents no symptoms, thus the only way to prevent blindness from POAG is early detection and consistent monitoring of progression of the disease, as well as the effect of medications.

Diagnosing POAG in Ghana is typically done by eye specialists using a method known as ophthalmoscopy, which involves examining the interior of the eye (the fundus) with a magnifying instrument. The challenge with this however is with the availability of experienced eye specialists, especially in rural areas where POAG is most prevalent.

This thesis employs the use of a relatively new type of Artificial Neural Network known as the Pulsed Coupled Neural Networks together with thresholding techniques and a simple multi-layer back propagation neural network to predict glaucoma from fundus images.

We propose a new algorithm for extracting key glaucoma prediction parameters – the vertical cup to disc ratio and the inferior superior nasal temporal rule assessment. The system then subsequently predicts glaucoma. A total of 166 fundus images from Soyuz Medical Imaging and Diagnostic Center in Accra, Ghana was analyzed by the department of optometry and visual science in KNUST by primary eye care specialists, and set as the standard for measuring the reliability of the algorithm. The system correctly extracted and measured the vertical cup-to-disk ratio with a root mean square error of 0.11. Further, it achieved a specificity of 91.4% and a sensitivity of 88.6%.

The system is thus reliable, and can be employed in a mass screening application.
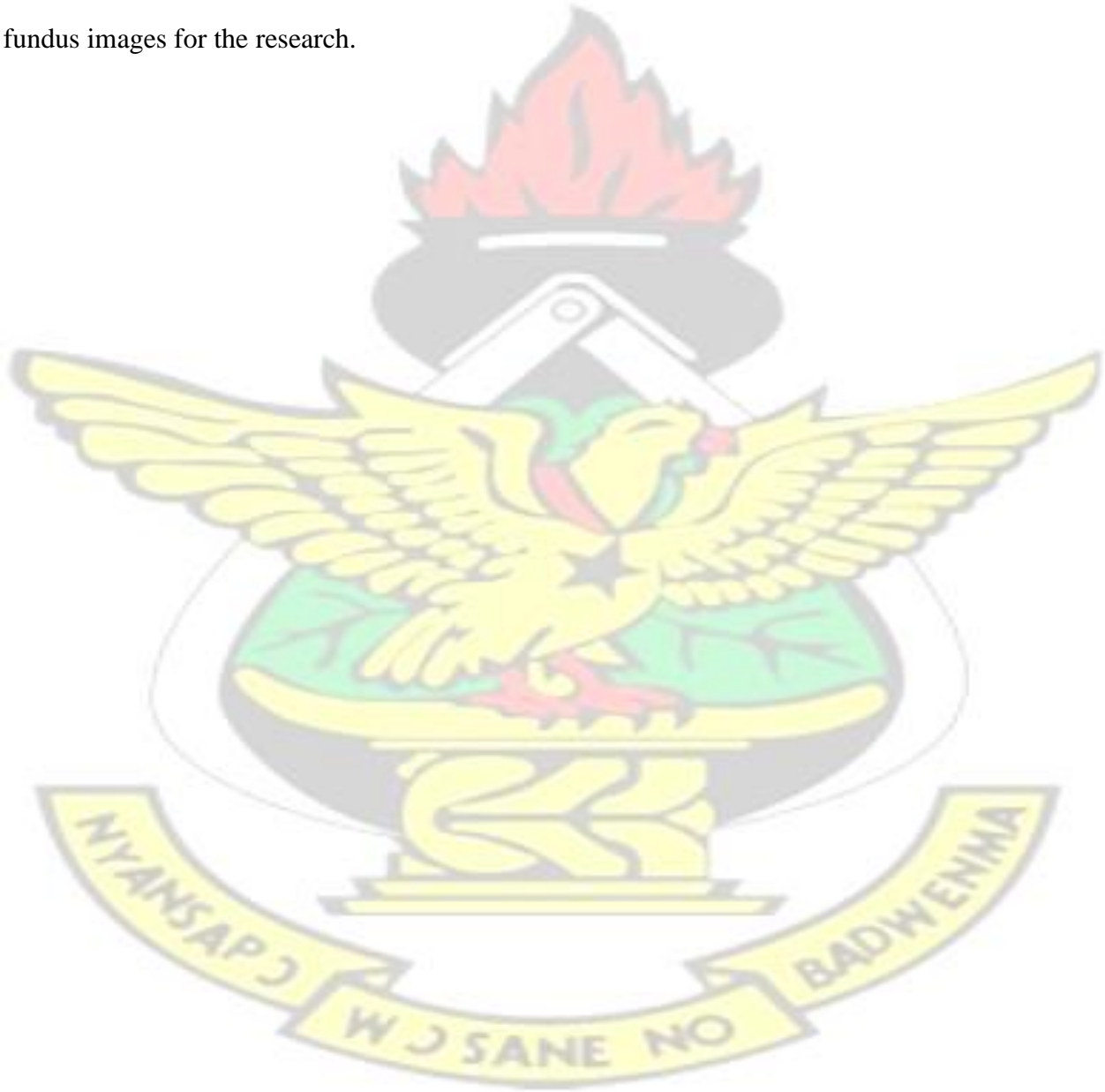
**DEDICATION**

This work is dedicated to the Almighty God, for His infinite grace and favor upon my life.

## ACKNOWLEDGEMENT

# LIST OF ABBREVIATIONS

| | |
|---|---|
| BPNN | Back Propagation Neural Network |
| CADx | Computer Aided Diagnosis |
| CDR | Cup to disc ratio |
| IOP | Intra ocular pressure |
| ISNT | Inferior Superior Nasal Temporal |
| NRR | Neuroretinal rim |
| OC | Optic Cup |
| OD | Optic Disc |
| ONH | Optic Nerve Head |
| PCNN | Pulsed Coupled Neural Network |
| ROI | Region of Interest |
| vCDR | Vertical Cup to Disc Ratio |
| VF | Visual Field |

# Table of Contents

# LIST OF FIGURES

# LIST OF TABLES

## CHAPTER 1

## INTRODUCTION

### 1.0 Background

### 1.0.1 Glaucoma Overview

Glaucoma is generic term that describes a family of conditions that damage a vital part of the eye known as the optic nerve. Its key feature is the specific structural abnormalities of the optic nerve head (ONH), and the associated loss of visual field (VF). The VF is the total area in which objects can be seen in the periphery, when you focus your eyes on a central point. The most significant risk factor for glaucoma is an increase in the pressure in the eye called Intra ocular pressure (IOP). The nemesis of glaucoma is blindness. Glaucoma is the leading cause of blindness among people of African origin and is the leading cause of irreversible blindness globally. Generally, it is known to be the second leading cause of blindness in the world [1] [2]. There are about 3 categories of glaucoma - primary glaucoma, secondary glaucoma and congenital glaucoma (section 2.1.3). Primary glaucoma is described as either open angle (Primary Open Angle Glaucoma –POAG) or closed angle.

POAG is discussed in this thesis due to the fact that over 70% of all glaucoma cases in Ghana is POAG [3]. Thus, the term 'glaucoma' as used in this thesis will refer to 'POAG'. POAG is described as '*the silent thief of vision*' as it usually presents no symptoms before onset of blindness. This feature of POAG makes it more dangerous than other ocular maladies like cataract which usually presents symptoms, as blindness resulting from cataract can be reversed unlike glaucoma.

# KNUST

In Ghana, about 8% of the population above the age of 30 are afflicted with glaucoma [2]. Currently, Ghana has a total of about 24,658,823 citizens [4]. Out of that number, 33.2% are above the age of 30 (over 8 million people).

This puts the estimated number of people who have glaucoma according to [3] around 640,000. These statistics are alarming as any country will have challenges developing when 33% of its active population is threatened with blindness.

### 1.0.2 Diagnosing Glaucoma

Although glaucoma cannot be cured, its progression can be slowed down by treatment which mainly entails decreasing the pressure in the eye. Timely diagnosis of the disease with progressive monitoring is therefore very important. It is important however to note that the diagnosis of glaucoma is not made on the basis of a single test, but rather on the basis of diverse sources of information and a combination of various test methodologies and technical tools. The various methods are summed up into two basic categories [5] [6]

- Accessing Risk factors for glaucoma – these risk factors include increasing IOP, advancing age, African origin, smoking habits, etc.
- An Eye Examination – Examining the pupil, ONH, IOP, anterior segment, etc.

There are a number of ways that may be employed to examine the eye for signs of glaucoma. The critical part of the eye to examine in glaucoma is the optic disc. Pathological findings of the optic disc are related to the disease stage of glaucoma, and mostly they are detected before a patient recognizes any significant loss in VF [6].

Traditionally in Ghana, optometrists and ophthalmologists use a method known as

ophthalmoscopy to observe the fundus and predict glaucoma. (*The fundus is the interior of the eye, opposite the pupil, in the retina layer*). Ophthalmoscopy, also known as funduscopy involves using a magnifying instrument (an ophthalmoscope) together with a light source to observe the fundus. The figure 1 shows what an eye specialist will see when he performs funduscopy examination.

In order to suspect glaucoma, the eye specialist examines the optic disc and optic cup regions on the fundus as shown below
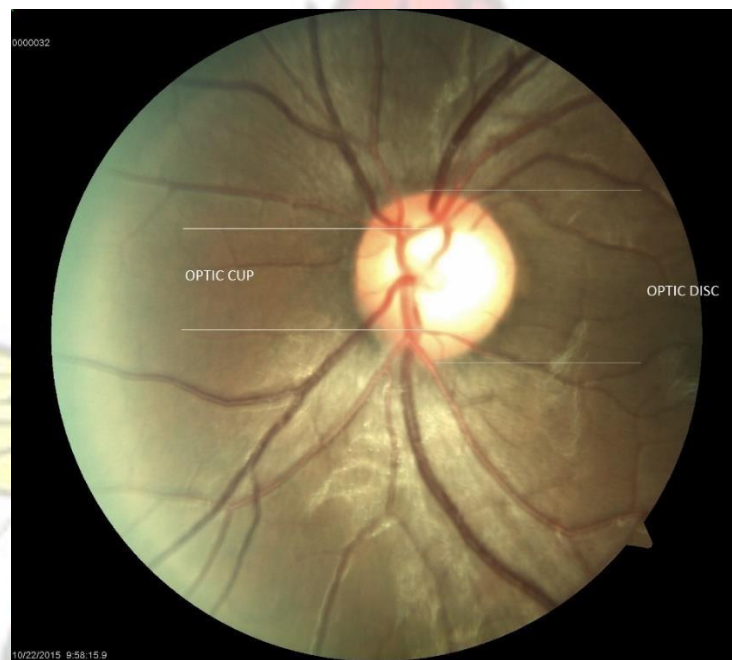


**Figure 1.1 A Typical Fundus Image Showing Optic cup and Optic disc**

The ratio of the optic cup to the optic disc, known as the cup-to-disc ratio (CDR) is a key clinical indicator sought for in the prediction of glaucoma. The CDR is usually calculated as the vertical cup-to-disc ratio (vCDR) as this is a more accurate clinical evaluation of the CDR. A vCDR is the measurement of the ratio of the vertical lengths of the optic cup and the optic disc. A high vCDR (the clinical term used is *cupping*) is usually (even though not conclusively) indicative of optic nerve damage.

Another key feature considered in glaucoma diagnosis via funduscopy is known as the Inferior Superior Nasal Temporal rule –ISNT Rule. The region between the optic cup and the optic disc is known as the neuroretinal rim (NRR). In a normal eye, the neuroretinal rim is broadest from the inferior, then superior, followed by nasal and then temporal region. In a glaucomatous eye, this rule is violated, and the superior region of the NRR begins to surpass the inferior region in terms of area. Thus, a vCDR is only dangerous and suspicious for glaucoma if it is accompanied by a violation of the ISNT rule. A high vCDR that obeys the ISNT rule is considered normal. The concept of cupping, and the ISNT rule is described in the figures 1.2 and 1.3 respectively.



**(a) Normal Cup**          **(b) Glaucomatous cup**

**Figure 1.2 Normal verses Glaucomatous ONH**

Thus to suspect glaucoma, vCDR and ISNT rule are two key parameters to check. Optometrists subjectively assess these parameters during funduscopy and then refer the patient for further tests including VF tests once any of these parameters are suspicious.
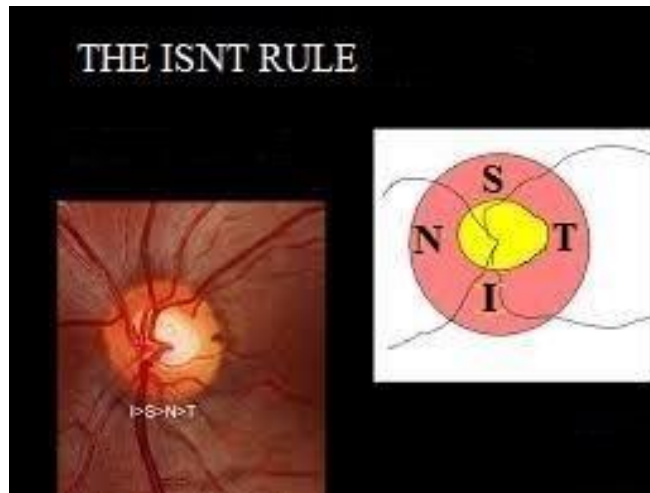
**Figure 1.3 ISNT RULE**

## 1.1 Problem definition

The scarcity of resources (both human and equipment) in most health institutions in Ghana hampers the early detection and monitoring of the progression of glaucoma in patients, resulting in avoidable cases of blindness.

Meanwhile, early detection and monitoring of the disease remains the only way to prevent subsequent blindness. Even though diagnosing glaucoma must result from consideration of information from multiple sources, the fundamental indicator sought for in diagnosing glaucoma remains the characteristic degenerative changes in the optic disc (vCDR and ISNT rule evaluation), and matching defects in the VF [6].

There is therefore the need to provide patients with a reliable system to help in predicting the occurrence or otherwise of glaucoma. Again, there is the need to provide eye specialists with an objective reference point, to reduce effects of fatigue and bias in analysing the fundus of patients and predicting glaucoma. This research aims to design a reliable image processing algorithm to help predict Glaucoma, with a mass screening potential.

**1.2 Statement of Objectives**

**1.2.1 General Objective**

The main aim of the research is to design a reliable image processing algorithm for a computer aided diagnosis system that can predict the occurrence of, and monitor the progression of glaucoma, with limited human intervention.

**1.2.2 Specific Objectives**

In order to achieve the set objective, the following specific objectives have been set

- Propose an algorithm to accurately measure the cup-to-disc ratio from the optic disc region of the fundus image

- Evaluate the violation or otherwise of the ISNT rule

- Automatically analyze extracted features from the region of interest (optic disc) and classify results as either suspicious for glaucoma or otherwise

**1.3 Justification of Research (Motivation)**

The prevalence of glaucoma in Ghana, coupled with the limited access to resources for eye disease management and treatment in Ghana makes such a tool indispensable for potential glaucoma patients. Sadly, many of the glaucoma cases were recorded in rural Ghana [3] where access to primary eye care was limited. Our vision is to deploy this algorithm in a cloud architecture that will provide easy and affordable access points for patients in rural areas using the already established telecommunication technology in Ghana. [7]

Again, this tool will prove indispensable to primary eye care specialists. It will alleviate the challenge of observer bias and fatigue by providing an objective reference point. It will provide a

reliable measure of the relevant parameters –vCDR and ISNT rule evaluation and then based on that predict glaucoma from fundus images.

## 1.4 Organization of Thesis

Chapter 2 of the thesis begins with an overview of ocular anatomy and physiology, and subsequently a look at the pathophysiology of glaucoma. We then review some ocular imaging modalities in the light of Computer Aided Diagnosis (CADx). We then examine some existing image processing algorithms. Later in the chapter, Artificial Neural Networks, and their applications in image processing is considered and the chapter ends with a description of Pulse Coupled Neural Networks and back propagation neural networks.

Chapter 3 introduces the proposed algorithm, and explains the various theories, assumptions and concepts employed in the design of the algorithm. Chapter 4 presents results and discusses findings from the algorithm as applied to a total of 166 images. Chapter 5 concludes on the work done, presents recommendations and proposes areas for future research.

## CHAPTER 2

## LITERATURE REVIEW

### 2.1 Overview of Glaucoma

In order to fully appreciate glaucoma, we review ocular anatomy and physiology and present the pathophysiology of glaucoma.

### 2.1.1 Anatomy of the Eye

The adult human eye is roughly spherical with a diameter of about 2.5cm (1 inch). From an engineering perspective, the eye can be modelled as a vessel with inflow and outflow channels that has the ability to regulate its internal pressure by controlling the rate of inflow and outflow. The eye is filled with intraocular fluid which exerts a pressure known as the IOP on the wall of the eyeball to keep it distended. The entire eye wall is composed of three concentric layers or *tunics*. From the inner to the outermost layers they are the *nervous tunic*, the *vascular tunic* and the *fibrous tunic*. Each of these tunics play a vital role in Glaucoma. Figure 2.1 shows the eye.
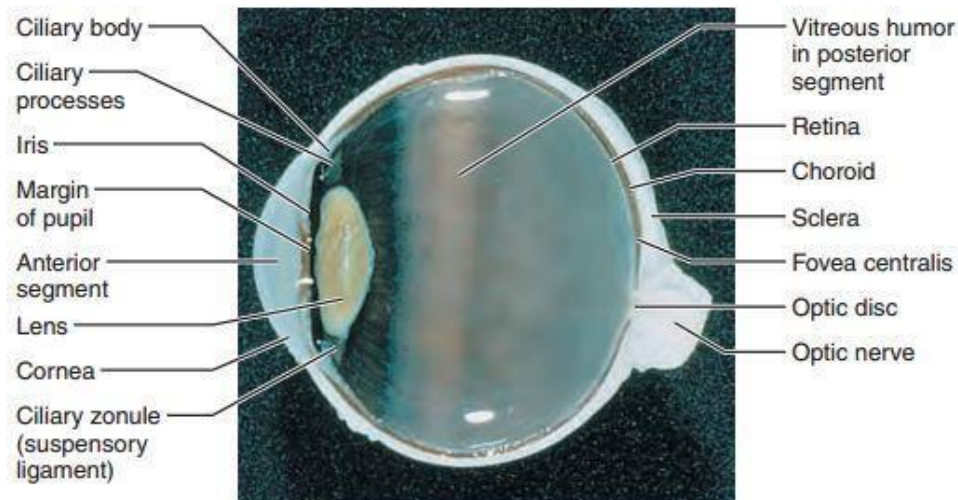
**Figure 2.1 The human eye**

## 2.1.1.1 The Nervous Tunic

The nervous tunic, also known as the retina, is the delicate innermost layer of the eyeball. It is an out-pocketing of the brain and contains millions of neurons. A neuron is basically an electrically excitable cell that processes and transmits information through electrical and chemical signals. A neuron is primarily made up of three parts – a cell body, a dendrite and an axon. Axons are elongated processes of neural cells along which information is transmitted by travelling electrochemical waves known as *action potentials*. Figure 2.2 below shows a typical neuron.
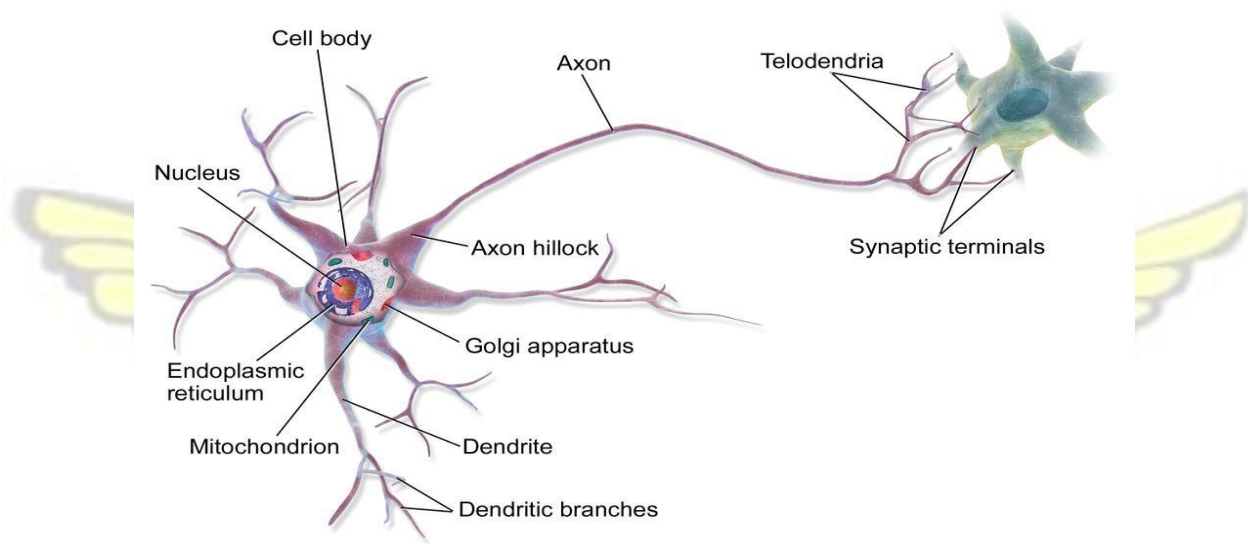


**Figure 2.2 A Typical Neuron Cell**

There are three main types of neurons in the retina - photoreceptors, bipolar cells and ganglion cells. Physiologically, signals are generated in response to light that enters the eye, and spreads from photoreceptors, to bipolar cells and then finally to the ganglion cells where action potentials are generated, and carried through their axons into the brain for interpretation. The axons of the ganglion cells turn at a right angle from the inner side of the retina, and then exit the posterior aspect of the eye as the thick optic nerve as observed in figure 2.5 .

**2.1.1.2 The Vascular Tunic**

The vascular layer is also known as *uvea*. It is pigmented, and has three sub-layers - choroid, ciliary body and Iris. The choroid extends anteriorly to form the ciliary body. The ciliary body is mainly smooth muscle bundles, and they control the shape of *the lens*. The lens focuses light onto the retina for image formation. Anatomically, the lens divides the entire eye into two main segments as seen in figure 2.3 below – the *anterior segment* and the *posterior segment*.
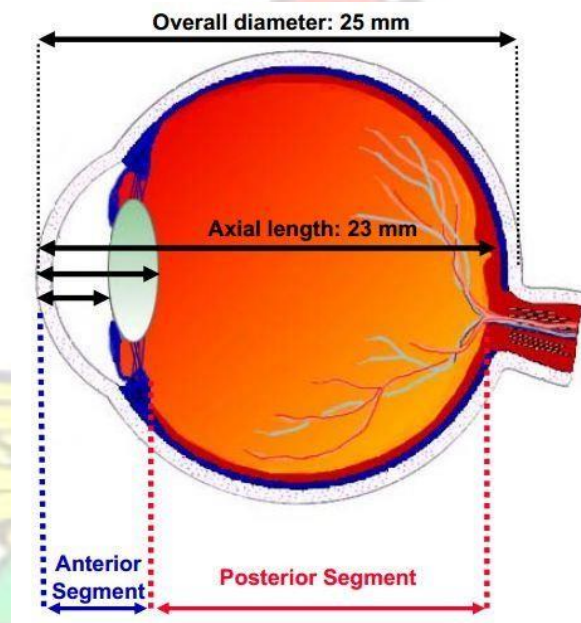


**Figure 2.3 Anterior and posterior segments**

The iris is the visible colored part of the eye, and the most anterior portion of the vascular tunic. It is shaped like a flattened doughnut, and lies between the cornea and the lens. It also divides the anterior segment into an *anterior chamber* and a *posterior chamber*. The iris has a round central opening called the pupil, which allows light into the eye. The iris controls the size of the pupil, and hence the amount of light that enters the eye. Figure 2.4 details the various divisions.
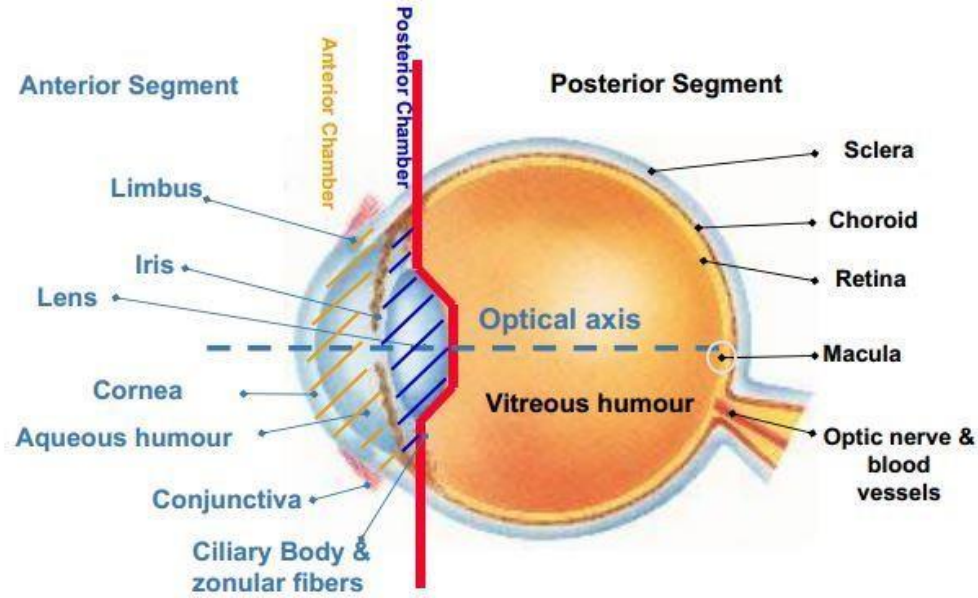
**Figure 2.4 Various Anatomical divisions of the eye –anterior segment, posterior segment, anterior chamber and posterior chamber**

### 2.1.1.3 The Fibrous Tunic

The outermost layer, also known as the *corneoscleral shell* is made up of two connective tissues – the cornea and the sclera.

The cornea is the major light bending apparatus of the eye. It is transparent, able to refract light and most significantly contain the IOP. It is made up of a protein known as collagen which gives the cornea its elasticity, form and strength. It forms about 70% of the total dry mass of cornea [8].

The sclera on the other hand, forms the posterior and bulk portion of the corneoscleral shell. It is glistening white and opaque, and it is this region we see anteriorly as the 'white of the eye'. The sclera is very stiff and is made up almost entirely of collagen. It is tougher than the cornea, and its main function is to protect the eye from mechanical injury, and contain the IOP.

The IOP imposes a pressure load normal to the inner surface of the eye wall, generating a circumferential stress known as the *Hoop Stress* [9]. This is borne by the fibrous tunic. Similar to

the other tunics of the eye, the corneoscleral tunic is pierced by the optic nerve posteriorly, and forms a thin netlike structure called the *lamina cribrosa.* The lamina cribrosa provides support and anchorage for the axons that pass through it, and serves as the reinforcement for the eye at its weakest spot.
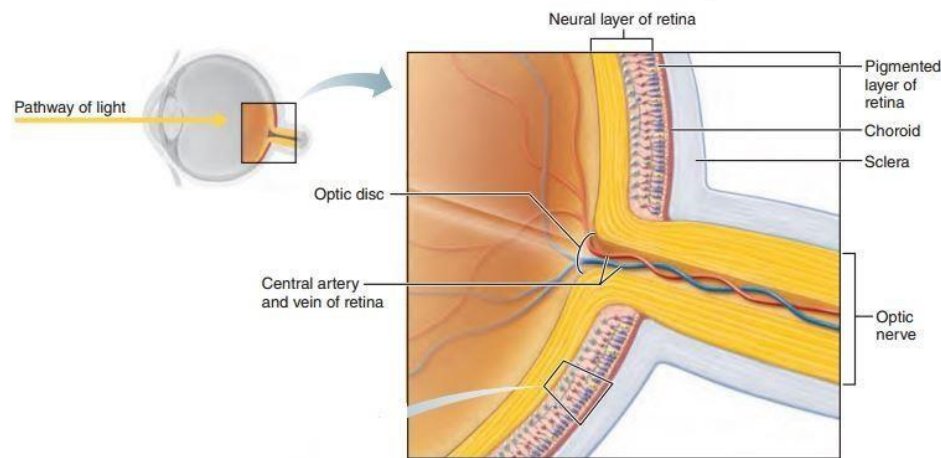


**Figure 2.5 Optic Nerve head**

The optic disc, also known as the optic nerve head (ONH) is most significant in the pathophysiology of glaucoma, as by definition, glaucoma is the death of the cells of the retina. In glaucoma, the IOP imposes an excessive compressive force on the OHN that mechanically assaults the axons of the retina cells.

**2.1.2 Pathophysiology of Glaucoma**

The fluids in the eye can be divided into two main portions – aqueous humor and vitreous humor. The aqueous humor lies in front of the lens (anterior segment), and the vitreous humor lies behind the posterior surface of the lens and the retina (posterior segment) as seen in figure 2.1. Aqueous is a free flowing liquid produced by the ciliary processes whereas vitreous is a gelatinous mass held together by a fine fibrillar network composed of elongated proteoglycan

molecules. Vitreous forms at the embryonic stage and lasts for a life time, whilst aqueous forms and drains continuously in the eye. Both water and dissolved substances diffuse into the vitreous, even though there is very little flow of fluid.

After formation of aqueous, it flows first as shown in figure 2.6 through the pupil into the anterior chamber of the eye. It then flows anterior to the lens and into the angle between the cornea and the iris, and then through a meshwork of trabecular and then finally through a canal known as the canal of Schlemm which empties into the extra ocular veins and then into the bloodstream. This accounts for about 90% of aqueous drainage. The remaining 10%, which constitutes a small but important proportion of aqueous drains across the ciliary body into the supra-choroidal space and is absorbed into the venous circulation (the uveoscleral pathway).

The outflow channels (meshwork of trabecular) have appreciable flow resistance, which coupled with the active production of the aqueous humor creates the IOP [10]. The amount of fluid leaving the eye by way of the canal of Schlemm is about 2.5µl/min, and equals the inflow of fluid from the ciliary body. IOP thus remains fairly constant in the normal eye, usually within 14-16 mmHg. The figure 2.6 summarizes this concept.
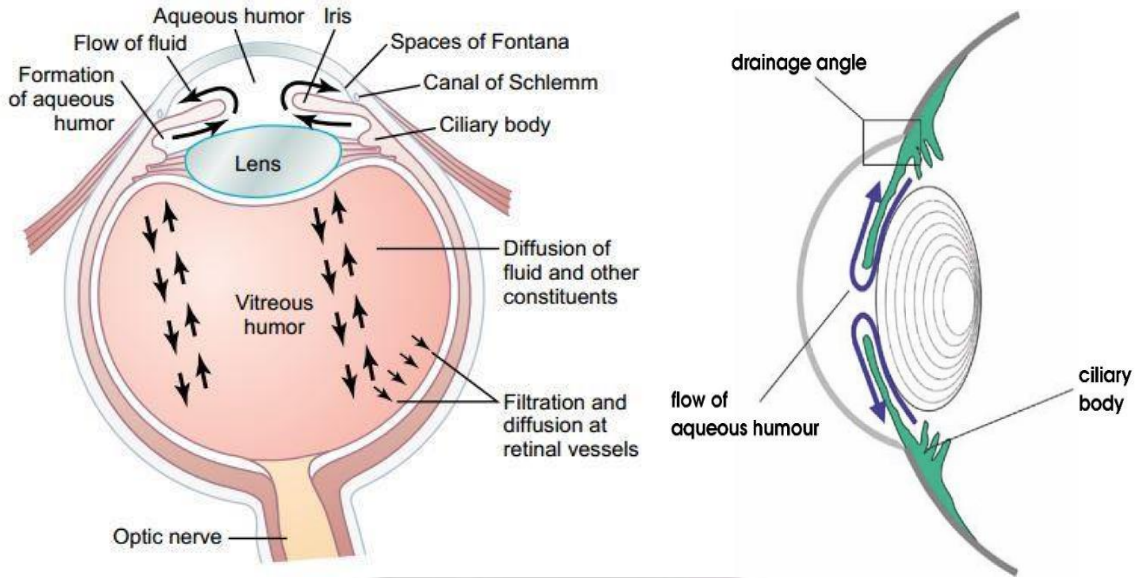
**Figure 2.6 Path of Aqueous flow, and IOP** [11]

The balance between the formation and drainage of aqueous regulates the total volume and hence pressure of the intraocular fluid.

In 2010, [12] proposed a model shown by equations 2.1 – 2.4 for IOP. The change in fluid volume in the anterior chamber of the eye can be described using conservation principles. For a time rate of change of anterior chamber volume (V) -

$$\frac{dV}{dT} = F_{in} - F_{out}$$

<div align="right">(2.1)</div>

$F_{in}$ represents the total rate of production of fluid volume by ciliary body, $F_{out}$ represents the rate of fluid volume loss from the eye via the trabecular meshwork. $F_{out}$ is described by equation 2.2.

$$F_{out} = \varepsilon C_{trab}(IOP - EVP) + F_u$$

<div align="right">(2.2)</div>

Where $F_u$ is the outflow via the uveoscleral pathway, EVP is the episcleral venous pressure, $C_{trab}$ is the facility of outflow via the trabecular pathway and the parameter $\varepsilon$ allows the varying of the

effective outflow facility to model diseased eyes. In the case of a healthy eye, $\varepsilon =1$. In the case of glaucoma, $\varepsilon$ can take on any value $0< \varepsilon <1$.

The change in volume from equation 2.1 can be related to the change in IOP using an empirical linear relationship from [11]. This is expressed as equation 2.3 where $K_r$ is called the mean ocular rigidity coefficient. Finally, equation 2.4 provides a link between IOP and fluid volumetric rate

$$K_r = \frac{d(IOP)}{dV}$$
(2.3)

$$\frac{d(IOP)}{dt} = K_r(F_{in} - F_u - \varepsilon C_{trab}(IOP - EVP))$$
(2.4)

In summary, optic nerve assault in glaucoma results ultimately from compressive forces from a rise in IOP that overwhelm the optic nerve head, and cause ischemia. The rise in IOP is caused by multifactorial variables, predominantly the resistance of the flow channels. The venous blood pressure may also affect the IOP as shown in equation 2.4. Ischemia is the termination or reduction of blood flow and hence oxygen access to a tissue or cell. Ischemia leads to the death of the ganglion cells, and over a period of time the gradual loss of vision.

### 2.1.3. Classification of Glaucoma

Glaucoma can be classified into three main categories [5]. This classification is based primarily on the mechanism by which aqueous drainage is reduced, leading to a rise in IOP. The classes are – Primary Glaucoma, Secondary Glaucoma and Developmental (Congenital [13]) Glaucoma.

In primary glaucoma, there is no other secondary or remote cause for the elevation in IOP. Classification of the primary glaucomas is based on the peripheral iris, whether it is:

- Open Angle ( clear of the trabecular meshwork )

- Closed Angle ( covering the trabecular meshwork )

In POAG, the obstruction is due to structural variations in the meshwork, while in closed angle glaucoma, the peripheral iris blocks the meshwork.

In secondary glaucoma, the elevation in IOP arises from systemic disease, drug use or other ocular disease. The cause of congenital glaucoma remains uncertain. The main hypothesis is that, there arise developmental anomalies in the anterior chamber angle (mainly the iridocorneal angle) during the embryonic stage. It is suspected to be covered with a membrane which increases the outflow resistance. [13] [5].

In Ghana and Africa at large, open angle glaucoma is predominant with over 70% of all cases being open angle in Ghana. [14]

## 2.2 Computer Aided Diagnosis (CADx) for Glaucoma

As discussed in the previous chapter, the traditional method for observing the fundus in Ghana is primarily ophthalmoscopy. Ophthalmoscopy is however not the only way to examine the interior of the eye. Technology has made it possible over the years to acquire images of the interior of the eye for subsequent examination. There are quite a number of ocular imaging modalities based on diverse technologies. The resulting images are useful for analyzing a wide range of pathological signs. The figure below summarizes some modalities [15] –
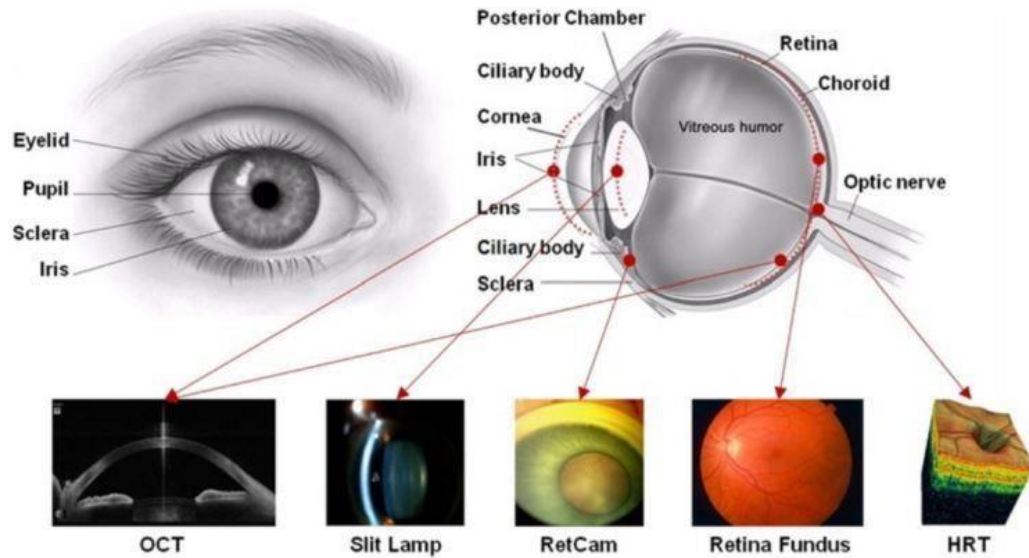
**Figure 2.7 Some ocular Imaging Modalities** [15]

An effective imaging modality for glaucoma is fundus photography. Fundus photography involves the use of a low powered microscope with an attached camera to capture color images of the fundus. It has an advantage over traditional ophthalmoscopy in that, there is a permanent record of the fundus that can be analyzed from time to time, and objectively compared with subsequent images to determine progression of glaucoma.

### 2.2.1 Image processing techniques and CADx

Over a period of two decades, development of image processing techniques that have direct applications in ophthalmology have paved way for the design and implementation of automated diagnostic systems for many diseases including glaucoma, since the research and development of CADx for ocular images begun around 1980s. CADx are systems that help clinicians in the interpretation of medical images by highlighting important aspects of the image. This generally improves speed and efficiency, in addition to causing significant savings in resources (human and non-human). Such systems also provide freedom from observer bias and fatigue. The first report

on retinal image analysis was published in 1973 focusing on vessel segmentation [16]. Eleven (11) years later, [17] also published a work on image analysis of fundus photographs. The focus was on detecting lesions related to diabetic retinopathy. CADx for ocular diseases have since enjoyed extensive attention from researchers and clinicians alike across the world. [15].

For effective CADx analysis, the image processing algorithms employed must be robust and effective. Image processing algorithms may be generally classified into six (6) different classes –

i.  **Pre-processing** – image pre-processing involves the processes performed on an image before the main image processing task is attempted. It usually aims at presenting the image in a more suitable condition for further processing. It includes techniques like contrast enhancement and smoothing the image.

ii. **Data Compression** – data compression is the processes of decreasing the size of an image without compromising on the quality of the image, usually to ensure convenient transmission of the image over a medium. The compression technique may be described as either lossy or lossless based on whether it is possible to obtain all the information in the image after decompression (as in the case of lossless) or not (as in the case of lossy.) iii. **Segmentation** - image segmentation involves the processes used to subdivide an image into constituent usually similar parts, or isolating certain portions of an image. They include shape detection, identifying objects, etc.

iv. **Feature Extraction** – feature extraction in image processing is the process of selecting derived values (features) from an image. These features must be unique, and must carry information. This information is usually used by some machine learning or pattern recognition method to automatically draw inferences about the image

v.  **Classification** – Classification in image processing is the process of categorizing pixels in a given image into one of a given class. Pixels that have similar properties are considered a class.

vi.  **Optimization** – Optimization in image processing involves techniques employed to compensate for missing or corrupted image data. It also involves the processing of finding similarities between two separate images.

As with many bio-signals, images obtained with current imaging modalities often require preprocessing to remove noise and enhance contrast before further analysis by CADx methods are applicable. Due to our set objectives, we focus our attention on Image pre-processing techniques (*preparing the image for effective cup and disc extraction*), Image segmentation techniques (*isolating the cup and disc for effective feature extraction*), feature extraction techniques (*selecting the relevant features –vCDR and ISNT rule evaluation for analysis and subsequent classification*) and classification techniques (*for categorizing features and hence images as either suspicious for glaucoma or not*) in the development of the proposed algorithm.

There are generally about five methods that have been used over the years to achieve the task of Image pre-processing, and thus preparing ocular images for CADx. [15]. They are –

a.  **The Histogram Equalization Approach** [18] [19] – This technique is basically an automatic way to achieve histogram stretching to enhance contrast in an image. A histogram shows the number of times each grey level in the image occurs in the image.

Histogram equalization balances the distribution of bright and dark pixels in the image, thus ensuring that a dark image is made brighter, whilst an image that is too bright is darkened appropriately.

b. **Shade Correction Approach** [20] [21] [22] – For most images, a total of 256 grey levels are used to represent information (thus, the range of black (0) – white (255)). Each pixel is then a shade of grey. Shade correction involves altering the representation of different grey levels. This results in an altering of the image resolution, and hence the image is made blur. This technique is generally not very useful in fundus color processing, even though in specific cases it may prove appropriate.

c. **Convolution with a Gaussian** Mask [23] – This technique is described in section 3.2.2.3. It is a low pass filtering technique, similar to the averaging filter approach. The objective with Gaussian filtering is to remove high frequency components (noise), thus the convolution with a Gaussian mask approach tends to blur the image.

d. **Median Filtering Approach** [24] – The median filter is an example of a non-linear spatial filter used in image processing. It is most effective for removing a kind of noise in images known as 'salt and pepper' noise. The salt and pepper noise is also known as impulse or binary noise. It is a degradation to the image caused by sudden disturbances in the image signal, and it appears as randomly scattered white and or black pixels over the image. The median filter replaces a noisy pixel value with one closer to its surroundings. The setback with median filtering is the fact that it can be slow.

e. **Blood Vessel Removal Technique** [25] – This technique is very popular in developing image processing algorithms for CADx of glaucoma. When attempting to measure the prediction parameters via utilizing the intensity variations of the cup and disc region of the image, blood vessels serve as noise and make it difficult to achieve accurate measurements. Generally, an image processing technique called '*closing*', described in section 3.2.2.2 is used to remove blood vessels in the image.

The techniques above have all achieved different levels of success. However, none is appropriate when applied in isolation. The solution has been to adapt hybrid algorithms that harnesses the strengths in each approach as proposed by [17].

**2.2.2 Some Existing Image Processing Techniques for CADx for Glaucoma Diagnosis**

A technique was proposed in 2010 by [26] based on what was called the Line Profile Algorithm. The algorithm presents a graph of the vertical cup-to-disc ratio (vCDR). Their algorithm is summed up in figure 2.8
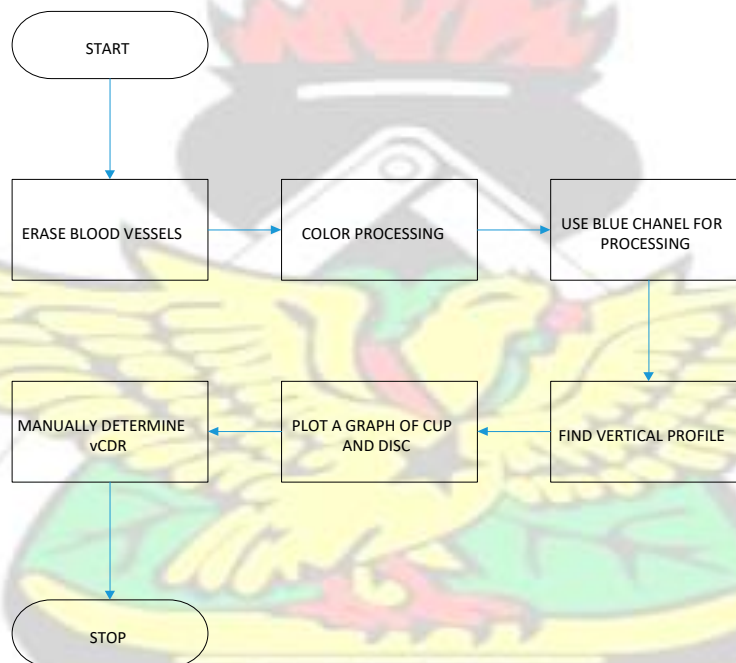


**Figure 2.8 Algorithm proposed by** [26]

First, blood vessels are erased from the image after the image is read into the system. The image is then split into its constituent red, green and blue channels.

The vCDR is able to examine the ISNT rule (check the inferior and superior NRR ratio) in addition to the cup to disc ratio. In glaucoma cases, the enlargement of the cup is usually in a vertical profile. According to the authors, the blue channel of the RGB image is extracted for further analysis due

to the level of high contrast between the optic disc (OD) and the optic cup (OC) regions in that channel as shown in figure 2.9a-3 and b-3.

A vertical profile of pixel intensities was then obtained along the center of the OD. The profile was a result of the average of 20 lines drawn through the middle point of the OD to the ear side of the OD on the left. This was done to ensure that the profile was not based on a specific line. Figure 2.9 outlines the entire idea. Figure 2.9a-1 and b-1 shows a fundus image with blood vessels. They are erased in a-2 and b-2 and then the blue channel is selected for the line profile analysis as seen in in a-4 and b-4.
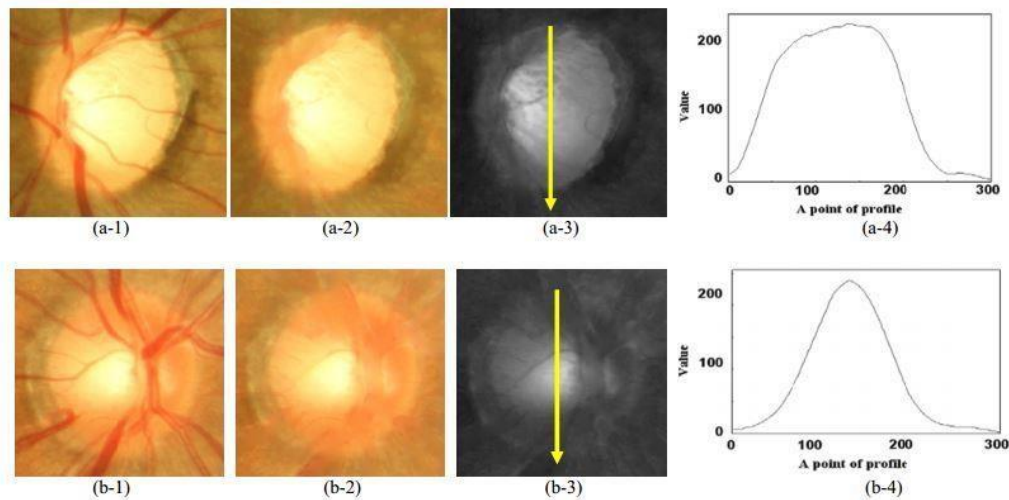


**Figure 2.9 The Line Profile Concept [26]**

The skirt region of the profile was determined manually as the neuroretinal rim region. It was determined by using an empirical threshold value of the profile. The CD ratio is then finally estimated using the cup edge and the disc region. Figure 2.10 summarizes this concept.
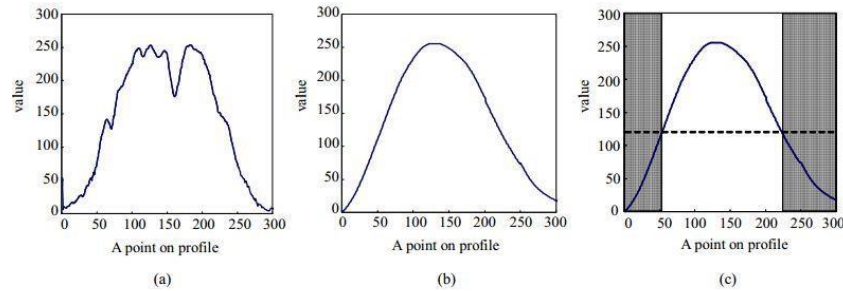
**Figure 2.10 – Determining the vCDR[25]**

Another algorithm was proposed in 2015 by [27], based on artificial neural networks (ANN) and the thresholding technique. The algorithm aimed to extract the CDR and evaluate the ISNT rule. Their algorithm is summarized below –
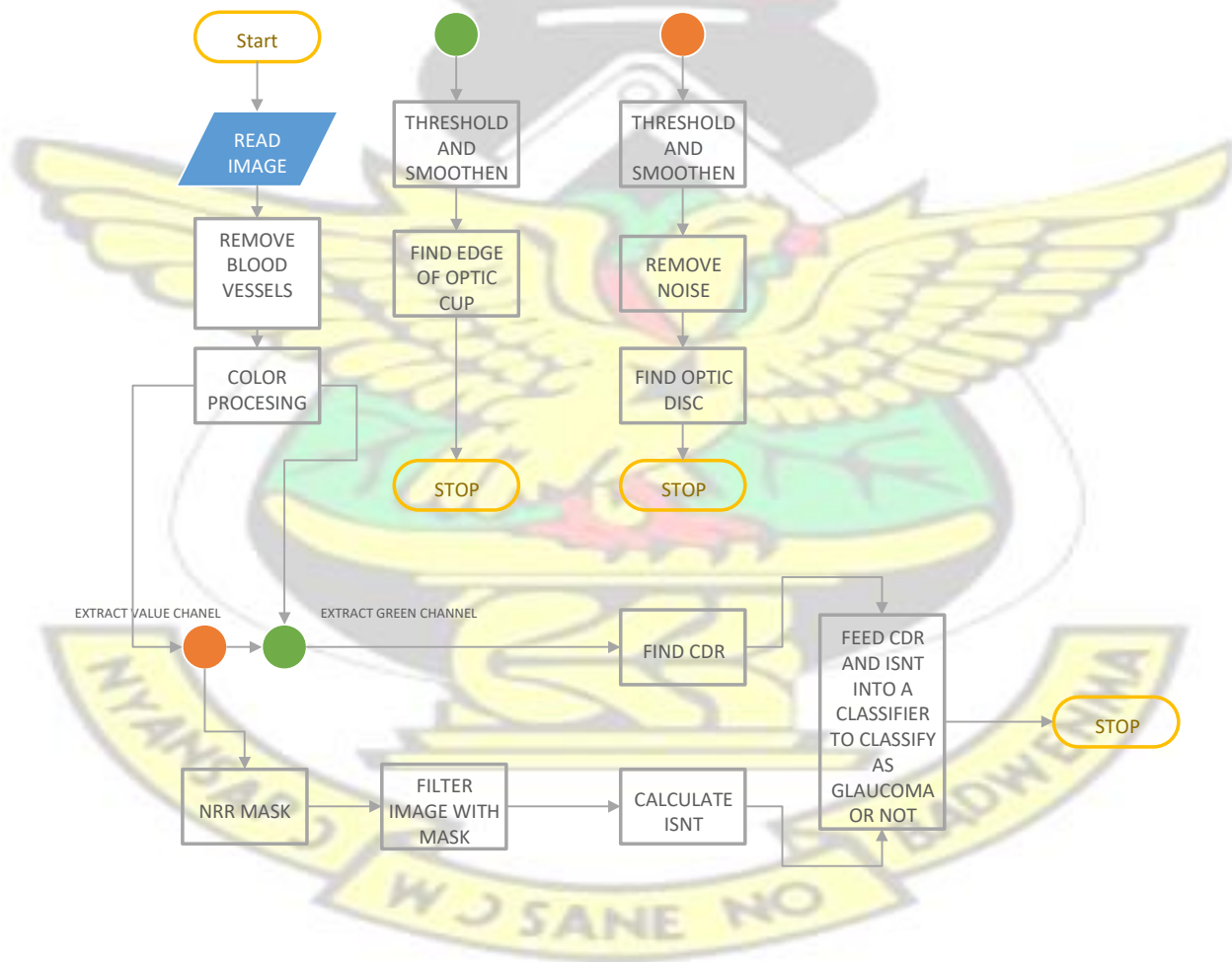
**Figure 2.11 High level view of Algorithm proposed by** [27]

First, the fundus image is read and cropped to focus on the OD region. The result is a 256 ×256 image. In order to evaluate the CDR, blood vessels are removed similar to the algorithm proposed by [26]. The image is then transformed into two color domains- the typical RGB color domain, and then the Hue, Saturation and Value (HSV) color domain. The mean value of the pixels in the V plane of the HSV color domain is calculated and set as the threshold for converting the image into a binary image. Noise is removed from the resulting image. A Gaussian filter is then used to filter the image to smoothen the boundaries of the image. This is summarized in figure 2.12



(a) Morphological operations

(b) V plane image

(c) Binary Image

(d) Gaussian filtered image
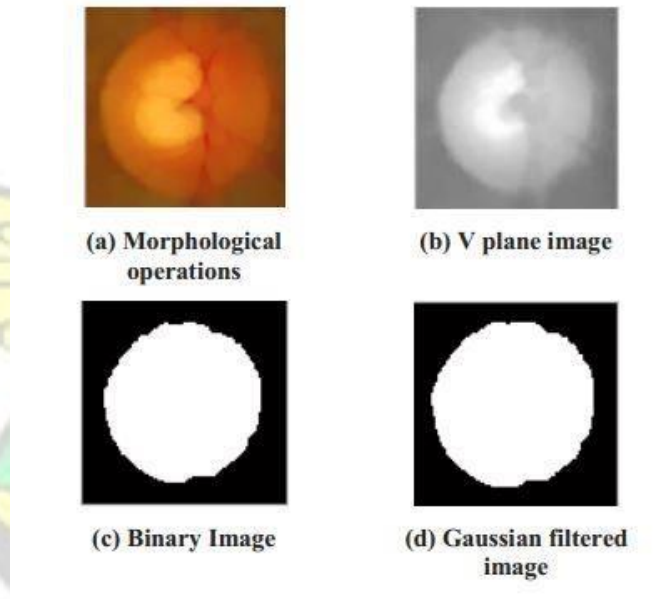
**Figure 2.12 Optic Disc Extraction by [27]**

To extract the cup, the green channel is selected. Based on the contrast between the cup region and the background in the green plane, a global threshold method was applied to segment the optic cup and create a binary image. The resulting image is then smoothened. The figure 2.13 shows the results of this procedure. The CDR is calculated as Cup Area ÷ Disc Area

(a) Green plane image        (b) Gray Image

(c) Gaussian filtered image
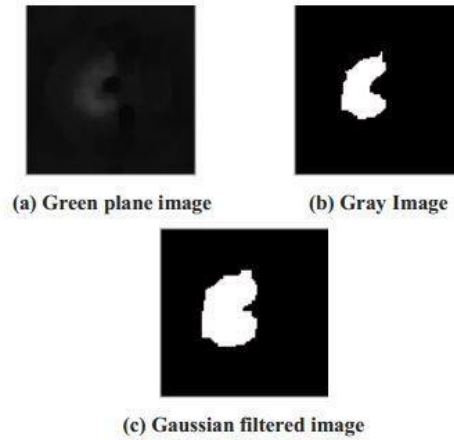
**Figure 2.13 Optic Cup Extraction Proposed by [27]**

The NRR region is calculated by subtracting the area of the OC from the area of the OD. To check the ISNT rule, a binary image of the NRR is taken and cropped.

A special mask of the same image size is used to filter one quadrant. The mask is then iteratively rotated 90 degrees to obtain the remaining 3 quadrants. Figure 2.14 shows the mask, and the ISNT rule evaluation procedure. The area covered by the white pixels is counted for the evaluation of the size of each I, S, N and T region of the NRR. Finally, 5 features – CDR, I quadrant pixel area, S quadrant pixel area, N quadrant pixel area and T quadrant pixel area are fed into a multi-layer back propagation neural network to classify as either glaucomatous or not.



(a)        (b)        (a) I quadrant        (b) S quadrant

(c)        (d)        (c) N quadrant        (d) T quadrant
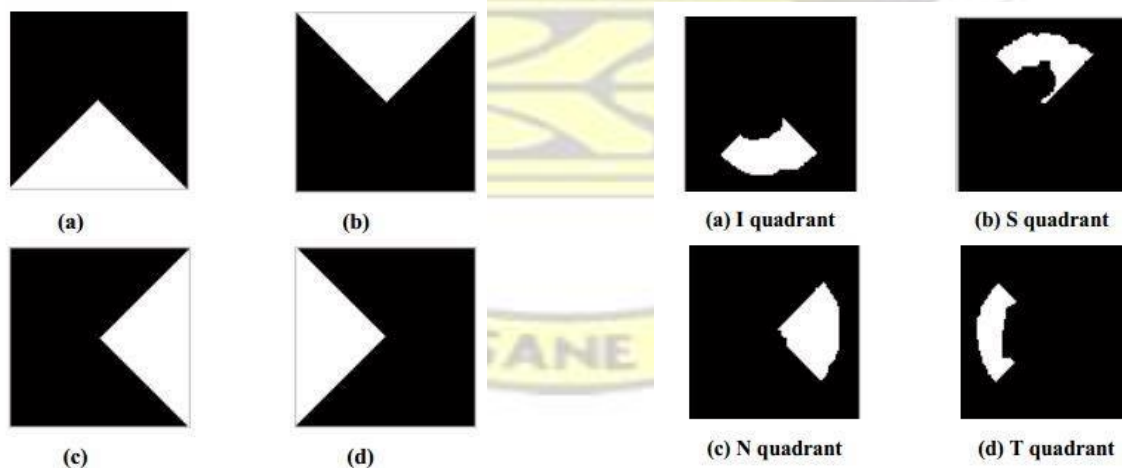
**Figure 2.14 Algorithm for ISNT rule evaluation proposed by [27]**

## 2.2.2.1 Problems with Proposed Methods

Even though there are challenges with both methods, they report some levels of success as discussed in chapter 4. The method proposed by [27] relies on the thresholding technique to segment the OC and OD. Thresholding depends on the quality of the image. The Thresholding methods employed in this case is most effective if the histogram of the given image is bi-modal. This is usually not the case, as a noisy V channel will cause the algorithm to fail in extracting the cup region. Again, the authors used the green channel for cup extraction. By observation, we realized that the green channel has the tendency to overestimate the cup size. The method proposed for calculating the cup to disc ratio and evaluating ISNT is based on counting white pixels in the image. This is prone to errors, especially when the preprocessing steps could not remove noise properly. In this scenario, white pixels in the image would be considered as part of the optic cup, or any of the I, S, N or T regions. Furthermore, clinicians estimate the vCDR not just the ratio of the cup size to the disc size. The mere ratio of cup size to disc size is not the accurate glaucoma prediction feature.

The line profile algorithm on other hand presents a graph for an eye specialist to analyze and decide what the vCDR is. Thus, the system is unable to automatically calculate the vCDR. The challenge of observer fatigue and bias still remains, for large scale screening in this scenario, as the eye specialist must manually determine the vCDR from so many graphs. These challenges must be met by introducing a pre-processing step before thresholding, which will ensure a bi-modal histogram distribution and thus proper segmentation of OD and OC, and then attempt to automate the estimation of vCDR.

In 2011, [28] reported promising results when they used a type of ANN known as Pulsed Coupled Neural Networks (PCNN) for texture segmentation. They applied PCNN as a preprocessing step, and achieved successful results. They concluded their study by recommending future work along the lines of employing PCNN for image segmentation tasks.

Not much attention has been given however to the use of PCNN despite their potential. According to their survey in 2012, [29] found out that only two works had been published where PCNN was used in image processing after [30] reviewed PCNNs and their uses in 2010.

### 2.2.3 Artificial Neural Networks in Image Processing

Generally, ANNs have proved their usefulness over decades in developing image processing algorithms that have found applications spanning different fields such as medicine, science, engineering, industry and security. [29]. It is worthy of note that since the 90's, when compared with other statistical methods, many studies have related advantages associated with applying ANNs. [31]

Artificial neural networks have become popular due to-

a. The fact that they are inspired by the nervous system.
b. Their usefulness for solving pattern recognition problems

c. Their parallel architectures

d. Their fault tolerance ability

### 2.2.3.1 Basic Structure of ANN

ANN techniques are generally a family of mathematical models, that take inspiration from the human brain functioning. The human brain is made up of billions of neurons, each with a limited processing power. However together, and working in parallel, the brain's processing ability is

extremely efficient. The brain is described by [32] as a highly complex, non-linear and parallel computer. It is this feature of the neurons and the brain as a whole, which informed the design and function of ANN. The first model of ANNs was known as the perceptron [33].

All ANN methodologies consist of 'neurons' in their designs. Each neuron is basically an *activation function* that controls the propagation of neural signal to other neurons connected to it. A neural connection has a *weight* that simply gives a measure of how strong the signal being conducted through it should be passed on to the next layer, similar to the synapse in the natural neural network. A positive weight stimulates the excitatory signal and a negative weight inhibits it.

A neural network is able to '*learn*'. The process of learning is the process of adjusting weights with the objective of mapping a given input to a specific output. There are several algorithms that have been developed over the years for the process of learning in ANNs. Generally, there are 5 methods – Error correction learning, Memory-based learning, Hebbian learning, Competitive learning and Boltzmann learning.

The most common and used learning algorithm is an error correction learning algorithm called the back propagation learning algorithm.

In order to utilize a neural network, it must be trained. Training a neural network is similar to the training process the human brain is taken through in order to acquire knowledge. Several inputoutput pairs (known as samples) corresponding to a class is fed into the network until the weights have been adjusted to ensure that the same kind of output is obtained for the same kind of input (This is known as supervised learning). At this level, the ANN is said to have been trained and is useful for classifying future inputs.

(A) Human neuron; (B) artificial neuron or hidden unit  (C) biological synapse; (D) ANN synapses.
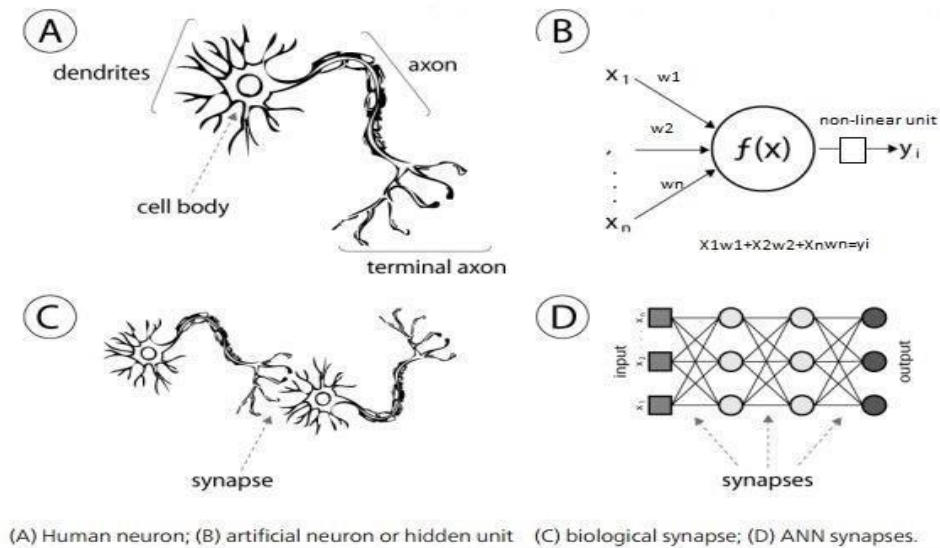
**Figure 2.15 The ANN and Natural Neural Structure** [31]

### 2.2.3.2 Types of ANN

There are several typical activation functions that constitute ANNs. Examples range from the simple threshold functions to linear functions, sigmoid functions and radial basis functions. The variations in activation functions may be used to classify ANNs.

The architecture, i.e. the neural connections, are also used to classify different ANN techniques. The so called feed-forward networks consist of unidirectional connections between network layers, i.e. connection flows from the input to the output with no feedback system. The recurrent or feedback ANN systems have connection patterns characterized by loops. This is due to the feedback patterns in this architecture. These different ANN architectures give rise to an intrinsically distinct behavior for each ANN topology. [31] Classifies ANNs based on–

   a.  Connection Patterns (Topology)

   b.  Number of neurons (hidden units)

   c.  Nature of activation function

d. Learning algorithm

According to [29], the following types of ANNs were most popular in image processing applications over the last decade –

i. Adaptive Resonance Theory (ART) ii.

Cellular Neural Networks (CNN) iii. Back

propagation Neural Networks (BPNN) iv.

Oscillatory Neural Networks (ONN)

v. Pulsed-Coupled Neural Networks (PCNN) vi.

Probabilistic Neural Networks (PNN) vii.     Radial

Basis Function Neural Networks (RBFNN) viii. Self-

Organizing Maps (SOM)

**2.2.3.3 Pulsed-coupled Neural Networks & Back Propagation Neural Networks**

Pulsed-coupled neural networks (PCNNs) are modelled after the visual cortex of some mammals. Its development started in the late 1980s when [34] found from studying the visual impression of the visual cortex of the cat that in the mid-brain, binary images were created in an oscillatory fashion from which the actual image is created.

In the early 1990s, other researchers confirmed similar findings in the guinea pig, and predicted its use in image processing algorithms [30]. It was in 1999 that it was modified and tailored for image processing algorithms [30]. As a new generation of neural networks, the PCNN is good for digital image processing, as the PCNN consists of a neuron per each pixel in the image.

On the other hand, the BPNNs are simple multilayer perceptron networks that employ the Back propagation learning rule. The BPNN is one of the most used learning algorithms in the domain of ANNs [31]. The main significant advantage of BPNN is the use of the output information and expected pattern to correct errors.

### 2.2.3.3.1 The PCNN Model

A good model for the PCNN was proposed by [29]. The PCNN architecture has three main modules – *the dendrite tree*, *the linking module* and *the pulse generator module* as shown in figure 2.16. The linking and feeding elements make up the dendrite tree, i.e. the input signal information is obtained through '*feeding*'. The linking and feeding elements feed information to the neuron element whiles the pulse generator module compares the internal activity $U(t)$ with a dynamic threshold to determine whether or not if the neuron should fire.

The PCNN module is summarized by equations 2.5-2.9 [28] [30].
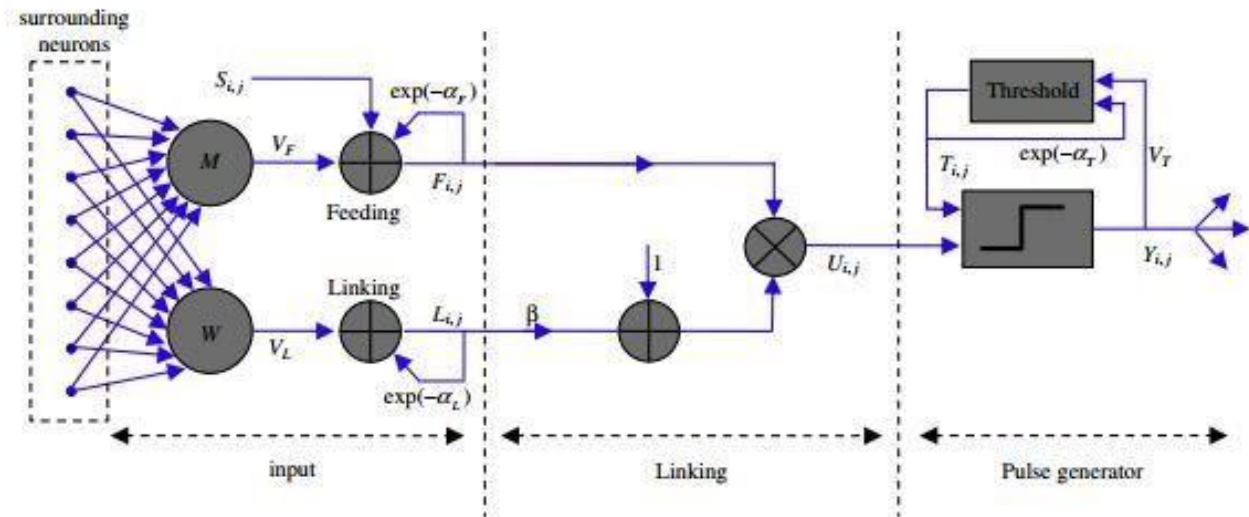
**Figure 2.16 The PCNN Model** [28]

$$F_{ij}[n] = e^{-a_F}F_{ij}[n-1] + V_f \sum_{k,l} W_{i,j,k,l} Y_{ij}[n-1] + S_{ij} \tag{2.5}$$

$$L_{ij}[n] = e^{-a_L}L_{ij}[n-1] + V_l \sum_{k,l} W_{i,j,k,l} Y_{i,j}[n-1] \tag{2.6}$$

$$U_{i,j}[n] = F_{i,j}[n]( 1 + \beta L_{i,j}[n])$$
(2.7)

$$Y_{i,j}[n] = 1 \ if \ U_{i,j}[n] > T_{i,j}[n], \ 0 \ otherwise$$
(2.8)

$$T_{i,j}[n] = e^{-a_T}T_{i,j}[n-1] + V_T Y_{i,j}[n]$$
(2.9)

Equation 2.5 represents the feeding region. $S_{ij}$ is the input pixel information. $a_F$ is known as the time constant of the leakage filter of the feeding region. $V_f$ is known as a potential. $Y_{(n)}$ is the neuron output at a given time (n), W is the feeding kernel.

Equation 2.6 shows the linking activity. $a_L$ is similar to $a_F$ but for the linking region, and M is the linking kernel.

Equation 2.7 describes the internal activity of the neuron element. This is a function of the linking and feeding activities. $\beta$ is the linking coefficient, and defines the measure of modulation of the feeding due to the linking activity. Equation 2.8 implements the dynamic threshold, where $a_\phi$ is the time constant of the leakage filter of the threshold and $V_0$ is the threshold gain. Equation 2.9 describes the output of the neuron.

2.2.3.3.2 BPNN

Back propagation algorithm is commonly used in conjunction with an optimization method such as the gradient descent algorithm [35]. The main idea of back propagation is to calculate the gradient of a loss function with respect to the weights of the network. The gradient is used by the

optimization method to update the weights in the network, with the objective of minimizing the loss function. The algorithm can be decomposed into four main levels –

a. Feed-forward computation

b. Back propagation to the output layer

c. Back propagation to the hidden layer

d. Weight updates

The back propagation algorithm requires that a desired output for each input is given, in order to calculate the cost function. It also requires that the activation function used be differentiable.

Consider a simple neural network with two input units and one output unit as shown in figure 2.17 below
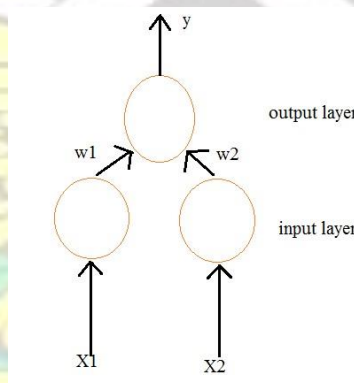


**Figure 2.17 A simple neural network model**

Let $(x_1, x_2)$ represent inputs into a neural network before training. Let $t$ be the correct output. Then *y* will be the output of the network with initial random weights. A common method for measuring the error between the expected output and the initial output of the network is the squared error ($E$) given by equation 2.10. The gradient descent method requires the calculation of the derivate of the squared error function, with respect to the weights of the network. Assuming only one input neuron, equation 2.10 becomes equation 2.11

$$E = (t - y)^2$$

$$(2.10) \quad E = \tfrac{1}{2}(t - y)^2$$

$$(2.11)$$

Let $O_j$ be defined as the output for each neuron $j$. Then equation 2.12 holds, where $net_j$ is the weighted sum of outputs $O_k$ of previous neurons.

$$O_j = \varphi(net_j) = \varphi\left(\sum_{k=1}^{n} W_{kj} O_k\right)$$

$$(2.12)$$

The variable $W_{ij}$ denotes the weight between the neurons $i$ and $j$. We use a logistic activation function described by equation 2.13 for each neuron. The derivative of the logistic function is then given by equation 2.14

$$\varphi(z) = \frac{1}{1 - e^{-z}}$$

$$(2.13)$$

$$\frac{d\varphi}{dz}(z) = \varphi(z)(1 - \varphi(z))$$

$$(2.14)$$

Using the chain rule, we find the partial derivative of the error with respect to a weight $W_{ij}$. This is given by equation 2.15. In equation 2.15, the term $\frac{\partial net_j}{\partial w_{ij}}$ is expressed as shown in equation 2.16.

$$\frac{\partial E}{\partial w_{ij}} = \frac{\partial E}{\partial O_j} \cdot \frac{\partial O_j}{\partial net_j} \cdot \frac{\partial net_j}{\partial w_{ij}}$$

$$(2.15)$$

$$\frac{\partial net_j}{\partial w_{ij}} = \frac{\partial}{\partial w_{ij}}\left(\sum_{k=1}^{n} w_{kj} O_k\right) = O_i$$

$$(2.16)$$

If the neuron in question is in the first layer after the input layer, then $O_i = x_i$. The derivative of the output of neuron $j$ with respect to its input is then given by equation 2.17. If the neuron is in the output layer, then $O_j = y$ and equation 2.18 holds.

$$\frac{\partial O_j}{\partial net_j} = \frac{\partial}{\partial net_j} \varphi(net_j) = \varphi(net_j)(1 - \varphi(net_j))$$

(2.17)

$$\frac{\partial E}{\partial O_j} = \frac{\partial E}{\partial y} = \frac{\partial}{\partial y}\frac{1}{2}(t-y)^2 = y - t$$

(2.18)

If on the other hand, $j$ is any neuron in a hidden layer of the network, $E$ can be considered as a function of the inputs of all neurons $L = u, v \dots w$ obtaining input from neuron $j$. Taking the partial derivative then becomes equation 2.19. Equation 2.20 shows the total derivative with respect to $O_j$

$$\frac{\partial E(O_j)}{\partial E_j} = \frac{\partial E\,(net_u, net_v, net_w)}{\partial O_j}$$

(2.19)

$$\frac{\partial E}{\partial O_j} = \sum_{l \in L}\left(\frac{\partial E}{\partial net_l} \cdot \frac{\partial net_1}{\partial O_j}\right) = \sum\left(\frac{\partial E}{\partial O_i} \cdot \frac{\partial O_l}{\partial net_L} W_{jl}\right)$$

(2.20)

Summing everything up gives us equation 2.21 with the condition expressed by equation 2.22

$$\frac{\partial E}{\partial W_{ij}} = \partial_j O_i$$

(2.21)

$$\partial_j = \frac{\partial E}{\partial O_j} \cdot \frac{\partial O_j}{\partial net_j} = \left\{ \begin{array}{l} (O_j - t_j)O_j(1 - O_j) \ \ if\ j\ is\ an\ output\ neuron \\ \left(\sum_{l \in L} \partial_l W_{jl}\right) O_j(1 - O_j)\ if\ j\ is\ an\ inner\ neuron \end{array} \right\}$$

(2.22)

The change in weight which is added to the old weight, is expressed by equation 2.23

$$\Delta w_{ij} = -\alpha \frac{\partial E}{\partial W_{ij}}$$

(2.23)

In the design of our algorithm, we employ the PCNN for image segmentation, and a BPNN for subsequent classification of input fundus images as either suspicious for glaucoma or otherwise.

**CHAPTER 3**

**ALGORITHM DESIGN**

## 3.1 Concept of Theory

To easily demonstrate the theory that this thesis presents, we use a simple analogy to show the task that the algorithm outlines for a computer to perform. Figure 1.1 shows what an eye specialist sees when he looks into your eye through an ophthalmoscope, what he is looking out for on the image and the anomalies on which to base his diagnosis.

The algorithm thus has the task of assuming the intelligence and expertise of the trained eye specialist to scrutinize the image and then predict the suspicion or otherwise of glaucoma by

noticing and extracting the OD, measuring the vCDR and checking for the consistency of the ISNT rule.

### 3.1.1 Experimental Setup

The algorithm is implemented in MATLAB R2013a, on a 64bit Intel® Core ™ 2 Duo CPU @ 2.20GHz with a RAM of 3GB PC.

A total of 166 Fundus Images were used for evaluating the algorithm. They were obtained from a Zeiss Visucam NM series fundus camera from a renowned eye clinic in Accra, Ghana. The department of optometry and visual science in KNUST manually marked outlines of the OD and OC, and classified the fundus images as either suspicious for glaucoma or not. This was set as the 'ground truth' and is used as the standard in the selection of parameters, and the design and testing of the algorithm.

### 3.2 Algorithm Design

The flow diagram below summarizes the entire algorithm proposed by this thesis. The algorithm basically has three major sections –

a. Image Pre-processing of Optic disc area

b. Extraction of prediction features

c. Classification of images as suspicious or not
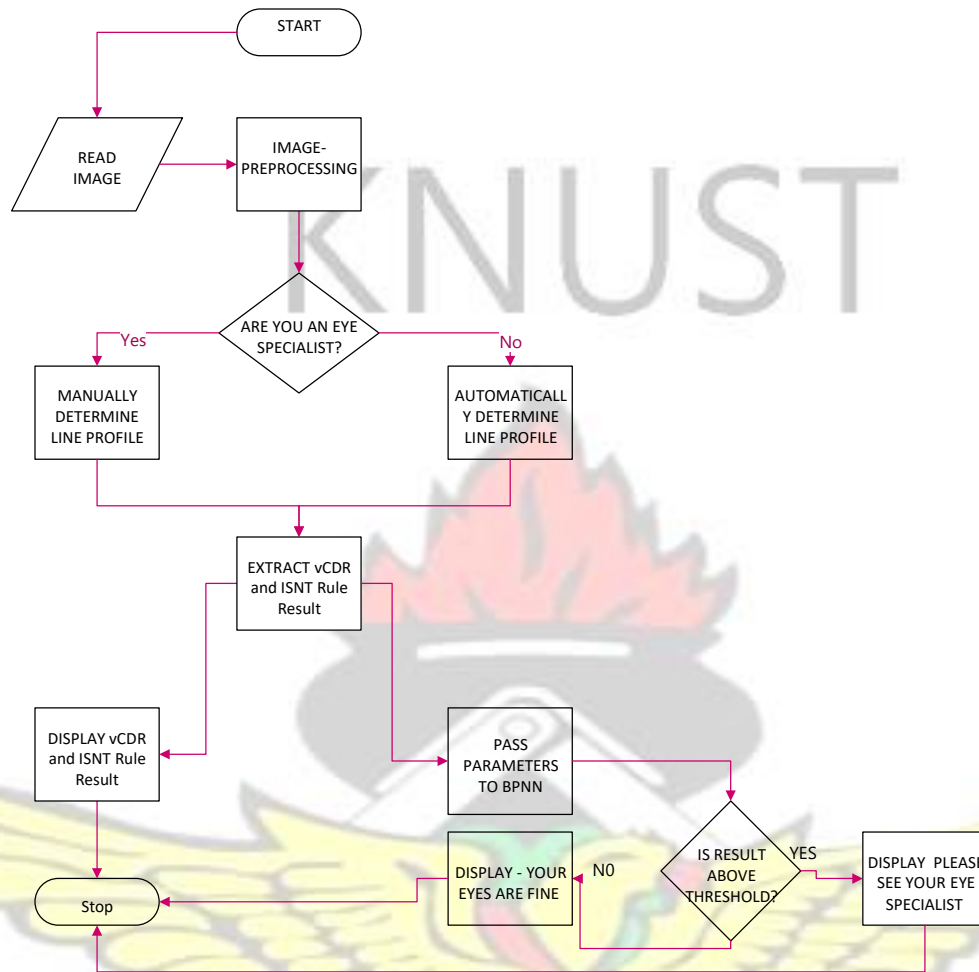
**Figure 3.1 Overview of proposed algorithm**

### 3.2.1 Reading the Image

As discussed earlier in section 2.2, there exists a plethora of imaging modalities for the acquisition of images of the eye for examination purposes. A fundus image is obtained primarily with a camera, aided by a low powered microscope.

In recent times, the rise in technological advancement has made it feasible to capture fundus images via mobile phones. [36]. Considering the prevalence of the telecommunications industry in Ghana, it is plausible to assume that fundus images can be acquired and transmitted to a central

CADx. Thus, the assumption this thesis makes it that fundus images are readily available. This study is focused on developing competencies for analyzing these images once they are have been presented to the system.

### 3.2.2 Pre-processing ROI

The pre-processing block of the OD region consists of 6 main sub-blocks – checking and storing image blurriness metric, removing blood vessels, color processing, removing noise, PCNN segmentation and then thresholding.
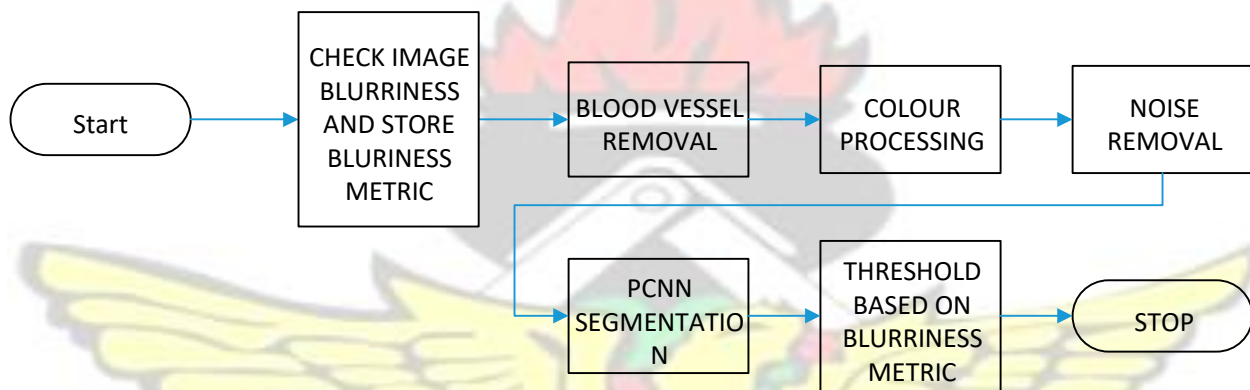


**Figure 3.2 overview of preprocessing block**

### 3.2.2.1 Checking For Image Blurriness

The algorithm begins by assessing the level of blurriness of the image. A method proposed by [37] is used. The technique involves the evaluation of the level of low frequency components in the image. The higher the low level frequencies, the more blur the image is. A blurriness metric is then stored containing the measure of how blur the image is. This informs what threshold value to use during the thresholding stage of the algorithm.

### 3.2.2.2 Removing Blood Vessels

The next stage is to remove blood vessels from the image. This is done by performing a closing operation. Closing is a type of image processing technique called morphology. A morphological operation is an image processing technique that is especially useful for shape extraction in images. There are two basic operations of morphology based on which all other higher operations are derived.

### 3.2.2.2.1 Dilation and Erosion

Suppose $A$ and $B$ are sets of pixels, mathematically, the dilation of $A$ by $B$ is defined as –

$A \oplus B = \{(x, y) + (u, v): (x, y) \in A, (u, v) \in B$. Thus, for every point $x, y$ which is an element in set $A$, we translate by $u, v$ which are elements in set $B$ and find the union of all these translations.

The erosion of $A$ by $B$ on the other hand is defined as $A \ominus B = \{w: Bw \subseteq A\}$

In both definitions, $A$ is the image being processed and $B$ is a kernel usually called a *structuring element*. A closing operation is a dilation operation, followed by an erosion operation. It is defined as $-A \blacksquare B = (A \oplus) \ominus B$.

Closing smoothens an image, fuses narrow breaks and thin gaps, and eliminates small openings. The operation was done using a disk structuring element of size 20. The result is shown in figure 3.3 below.
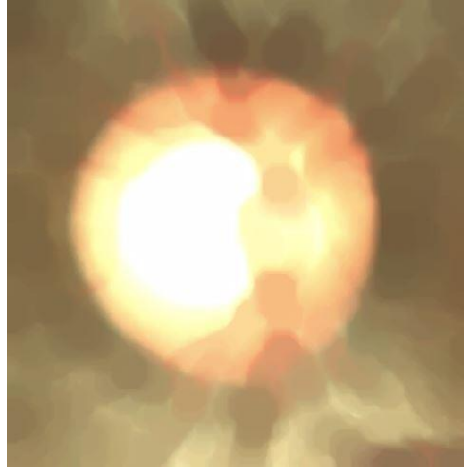
**Figure 3.3 Blood Vessel Removed From ROI**

### 3.2.2.3 Color Processing

The concept of color in image processing can be modeled in several ways. A color model is a way of specifying colors in a standard manner. The model adapted for use on computer screens is known as the Red Green Blue (RGB) color model. In RBG color model, a color is the result of varying amounts of red, green and blue. These colors are known as the primary colors, as the human visual system tends to perceive color as being made up of varying amounts of the primary colors. This is due to the nature of the cone cells in the retina.

Splitting the fundus color image into its constituent channels – Red, Green and Blue highlights contrast as seen in figure 3.4 The OD and OC regions usually have pixel values higher than the surrounding pixels. This contrast is highlighted in the various channels of the color image once the image is split into the various color components.

| (a) Red | (b) Blue | (c) Green |
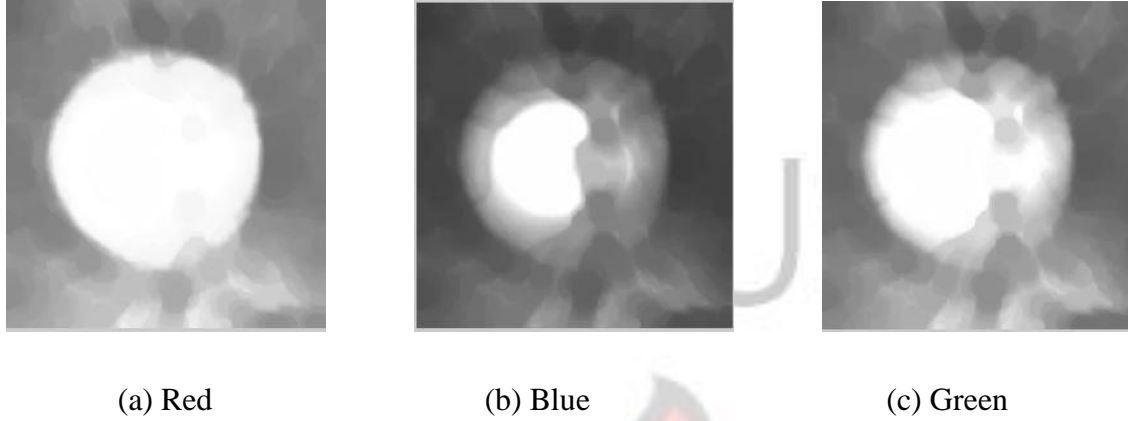
**Figure 3.4 RGB Color Channels of Fundus Image**

Based on experimental results, it was observed that the red channel presented a better contrast for OD segmentation. Even though the green channel presents a good contrast for the OC, there is the tendency of over estimating the size of the cup. The blue channel is thus selected for OC segmentation.

**3.2.2.3 Gaussian Filtering**

The image is smoothened to decrease noise. This is achieved by using a Gaussian filter. Gaussian filtering is described as a kind of spatial filtering. Spatial filtering is the application of a function to a neighborhood of each pixel in an image. The concept is that of moving a 'mask' (usually a rectangle with odd length of sides) across the entire image.

A filter is a combination of a mask and a function. Gaussian filters are a class of '*low-pass filters*' based on the Gaussian probability distribution function as shown in equation 3.1 and 3.2 for a 1D and a 2D dataset respectively where $\sigma$ is the standard deviation.

$$f(x) = e^{\left(-\frac{x^2}{2\sigma^2}\right)}$$

(3.1)
$$f(x,y) = e^{\left(-\frac{x^2+y^2}{2\sigma^2}\right)}$$

(3.2)

The frequencies of an image are the amounts by which grey values in the image vary with distance. A high frequency component is characterized by sharp changes in grey values over small distances, whiles low frequency areas are characterized by very small changes in grey values over large distances. High frequency components include noise and edges, whiles low frequency components include background and textures. Gaussian filters have a blurring and smoothing effect on the image, thus decreasing noise. This is useful in preparing the image for segmentation.



**(a) Gaussian filtered Blue Channel**                **(b) Gaussian filtered Red Channel**

**Figure 3.5 Gaussian Filtering**

### 3.2.2.4 PCNN and Thresholding

The filtered blue and red channels are fed as inputs into a PCNN. A good implementation of the PCNN was implemented in MATLAB by [38]. Each input pixel from the image corresponds to one neuron in the PCNN. An output pixel value is determined by the value of the surrounding pixel values in the image. The result is the segmentation of pixels that are similar, in this case the cup and disc on the blue and red channels respectively. This is seen in figure 3.6
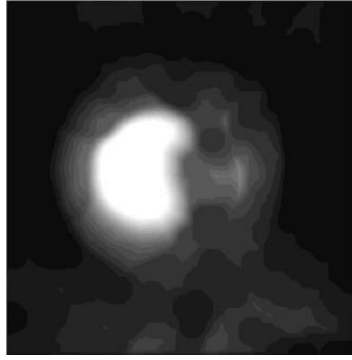
**(a) Optic Cup Segmented by PCNN**          **(b) Optic disc segmented by PCNN**
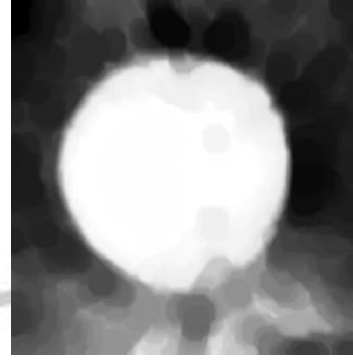
**Figure 3.6 After PCNN Processing**

At this stage, the images are ready for thresholding. Thresholding is a pre-processing step to convert an image into a binary format. A binary image is an image with pixel values having a value of either 1 (white) or 0 (black). A value T is computed for which the function *f(x)* is described equation 3.3

$$f(x) = \begin{cases} 1 \ if \ x > T \\ 0 \ if \ x \leq T \end{cases}$$

$$(3.3)$$

Specifically, a thresholding algorithm known as the Otsu's thresholding algorithm is used. Otsu's algorithm assumes that the image contains two classes, i.e., it follows a bi-modal histogram. It calculates the optimum threshold separating the two classes – foreground and background. The technique ensures that their combined spread is minimal by minimizing the weighted sum of the variance of the two classes. A modification to Otsu's method is what is called the double thresholding method. The double thresholding method finds two values of *T*, which separate the image pixels into background and foreground.

After the double thresholding algorithm is applied, two threshold values $-T_1$ and $T_2$ are calculated.

If the image is blur then the lower threshold is selected and used as the threshold for the conversion of the image into a binary format. If the image is not blur however, then the higher threshold is used to convert the image into binary.

The double thresholding algorithm produces the images in the figure 3.7 after PCNN has been used to prepare the images.



**(a) Optic cup**           **(b) Optic disc**
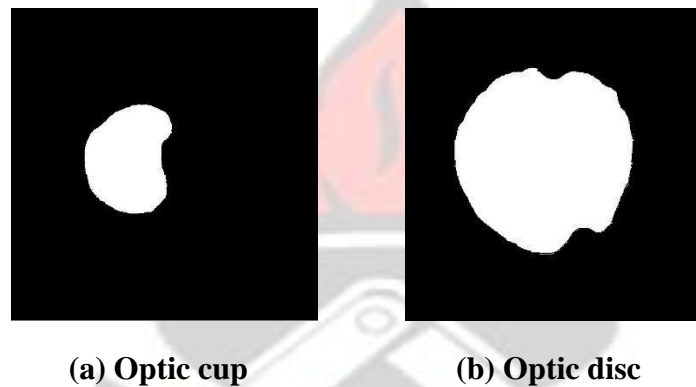
**Figure 3.7 Segmentation of Cup and Disc after Thresholding**

The resultant images for both cup and disc are merged to form one image. This is shown in figure 2.23a. The resulting image is then converted into an intensity value image with three distinct pixel values - 0, 150 and 250 (figure 2.23b). Zero (0) corresponds to the black background pixel values. The pixel values of 150 correspond to the gray neuroretinal rim area, whilst the pixels of value 250 correspond to the white pixels of the optic cup region. This is shown in the figure 3.8 below -



**(a)**                     **(b)**
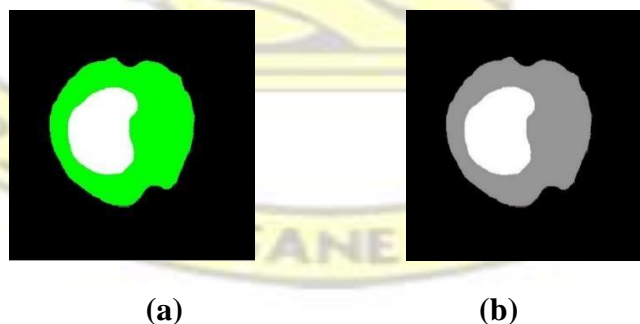
**Figure 3.8 Extracted Cup and Disc (a – color image, b – Grayscale image)**

## 3.2.3 vCDR and ISNT Rule Feature Extraction (AA algorithm)

To measure the cup-to-disc ratio and check the ISNT rule, we propose a new algorithm based on the concept of the Line profile algorithm from [26]. As stated in section 1.3, the algorithm will be used mainly by two groups of people – eye specialists and patients. A high level view of the algorithm is presented below in figure 3.9
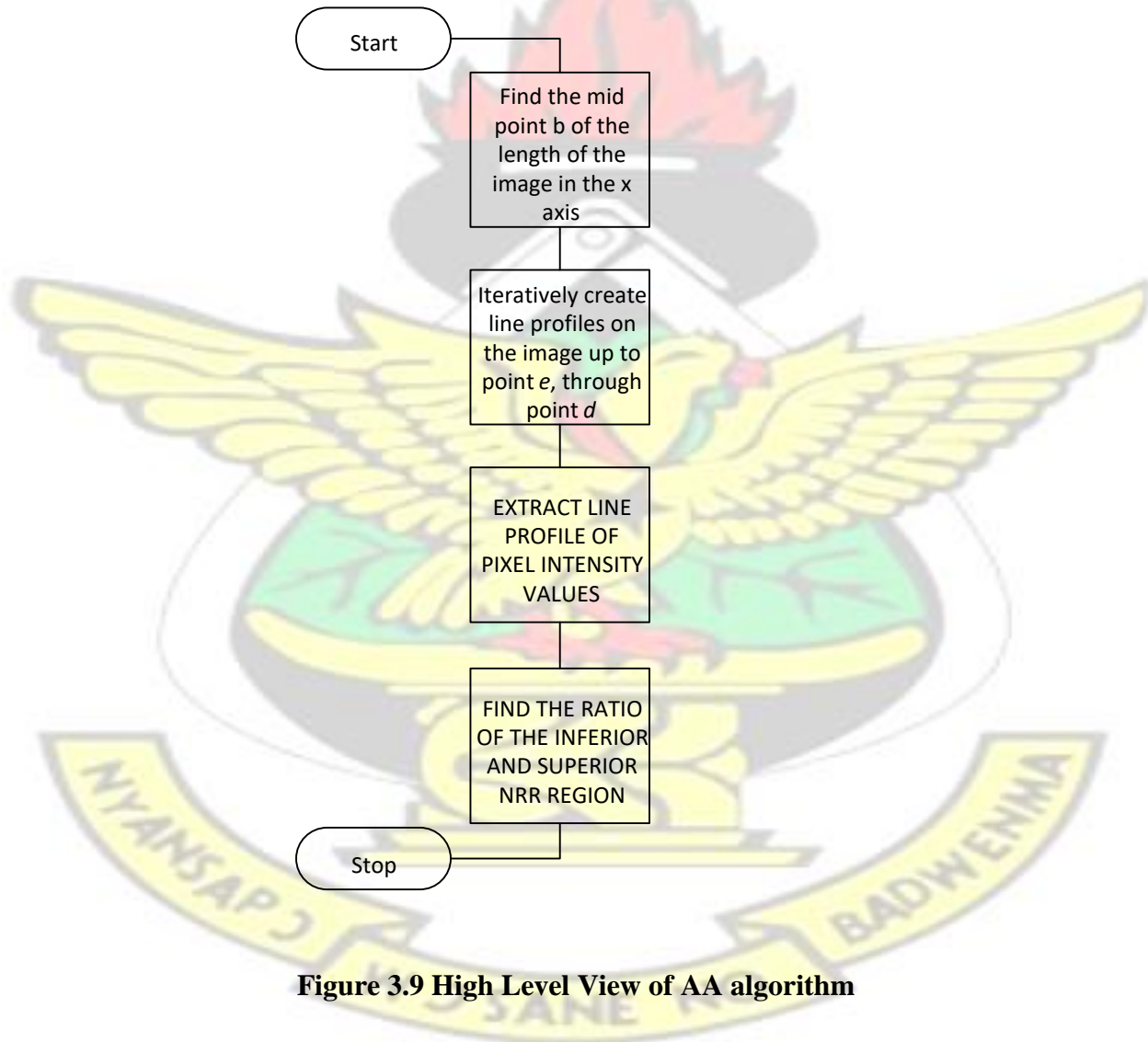


**Figure 3.9 High Level View of AA algorithm**

The algorithm presents two modes for extracting and evaluating the vCDR and the ISNT rule.

In the first mode, the pre-processed image is presented to the eye specialist, so that a vertical line is manually drawn on the image. The algorithm then automatically calculates the vertical ratio of the cup to disc based on the manually drawn line and presents an evaluation of the ISNT rule in terms of the ratio of the inferior to the superior NRR.

In the second mode, the algorithm automatically determines a vertical line and extracts the pixel intensities along that line. It then calculates the vCDR and presents a ratio of the Inferior region to the Superior region of the NRR.

To determine an appropriate vertical line profile, the image is considered in the XY plane as shown in figure 3.10
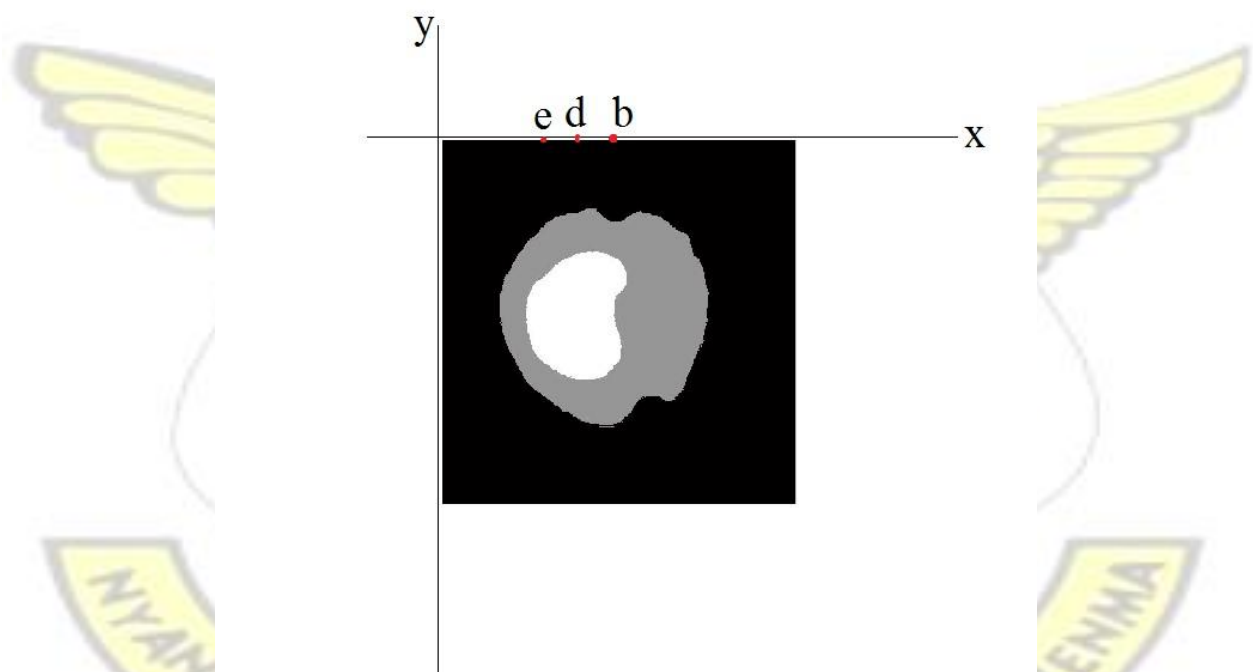


**Figure 3.10 Image in XY plane**

To determine point $b$, we find the pixel that corresponds to the location half the entire length of the image on the x axis. Using that as a starting point, we draw a line from top to bottom. We then estimate the Inferior and Superior NRR ratio. The process is repeated iteratively for points $b$-1, $b2$

*… b-n* through points *d* up to point *e*. The final line used for further analysis depends on the line profile that presents the largest length of the OC.
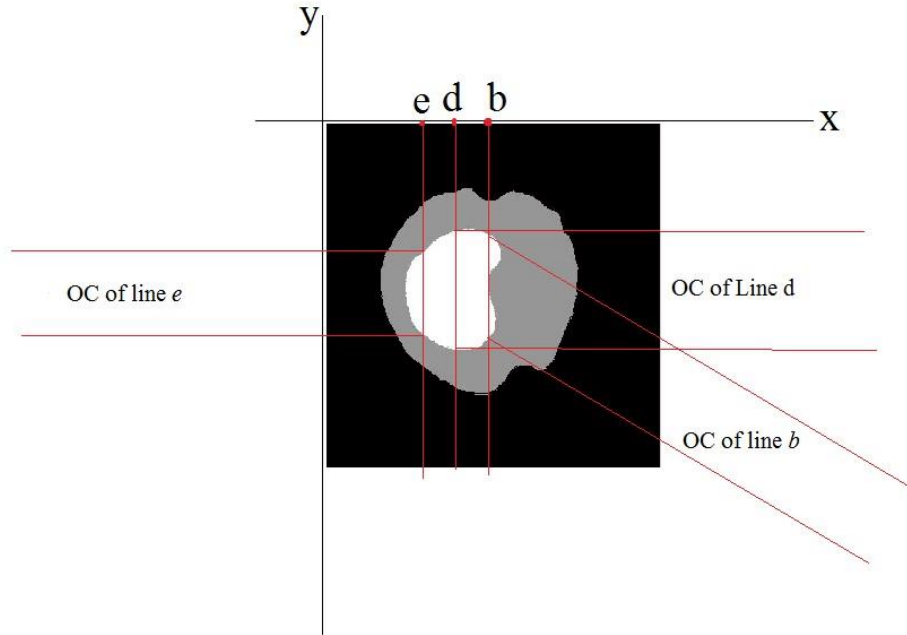


**Figure 3.11 Intensity Profiles**

**3.2.3.1 Determining the Cup and NRR from Intensity Profiles**

The pixel values from the vertical (*top to bottom*) intensity profile measurements are stored as matrix *A*. The matrix *A* has the form -

$$A = [a_{ij} \quad a_{(i+1)(j)} \quad a_{(i+2)(j)} \, a_{(i+n)(j)}]^T$$

The first *x* elements and the last *y* elements of the matrix *A* correspond to the dark background of the image, and is tagged as *noise*. It is not used in subsequent analysis. The figure 3.12 explains this more.
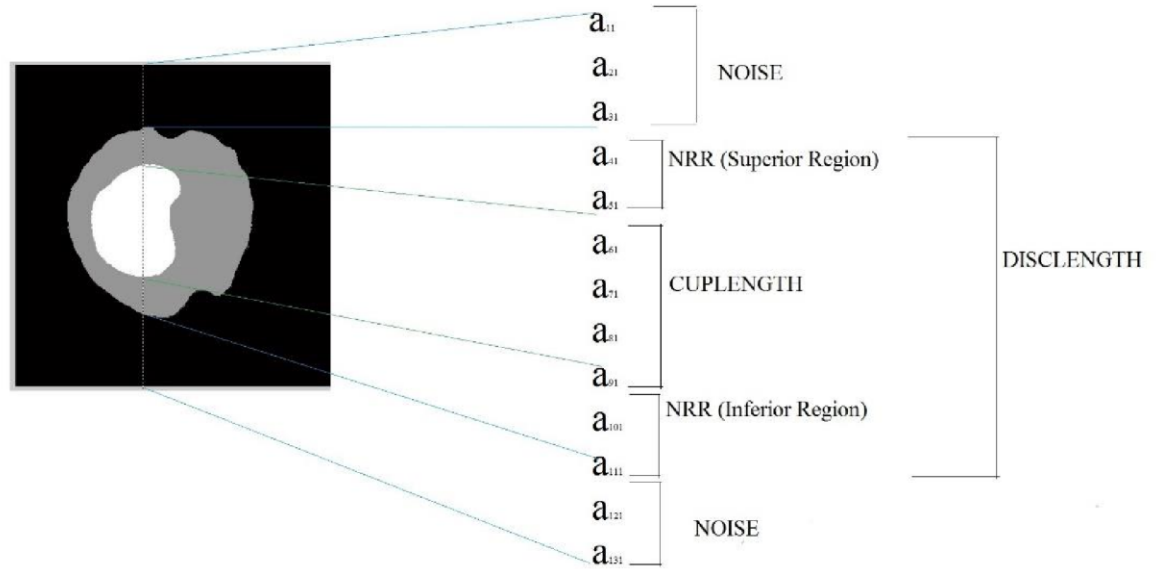
**Figure 3.12 vCDR, Superior and Inferior nrr**

The non-zero pixel values of matrix $A$ represents the vertical profile of the optic disc. A new matrix, $A_{disc}$ is thus created from $A$. $A_{disc}$ consists of only the non-zero values of A. The length of $A_{disc}$ is the vertical length of the optic disc, and is stored as *disclength.*

The maximum value $A_{max}$ in $A$ represents the values of the optic cup region. These pixels are extracted from $A$ to form a new matrix $A_{cup}$. The length of $A_{cup}$ is the vertical length of the optic cup, and is stored as *cuplength.*

The elements of matrix $A$ that are greater than 0, but less than $A_{max}$ represents the NRR of the OD region. This is extracted and stored in a new matrix $A_{nrr}$. The length of $A_{nrr}$ is stored as *nrrlength.* $A_{nrr}$ is of the form -

*[1+a, 1+ (a+1), 1+ (a+2) ... 1+p, 1+ (p+1), 1+ (p+2) ...] where p >> than a, and a $\geq$ 0*

*P is equal to the vertical length of the optic cup.*

The mean of $A_{nrr}$, $m$, is the pixel value that divides the elements of matrix $A_{nrr}$ into two distinct classes. The pixel values less than $m$ are extracted and stored as *SQ*. The length of *SQ* corresponds to Superior NRR length. The inferior NRR length is calculated as *nrrlength -length (SQ)*.

A feature set *F* is finally formed consisting of vCDR and Inferior region length /Superior region (IFL/SRL) - ***F = [vCDR, IRL/SRL]***

### 3.2.4 Predicting Glaucoma

The result of the extraction step is matrix *F*. *F* is fed as inputs into a multilayer BPNN. The set $F_{gluc}$ and $F_{norm}$ represents glaucomatous and non-glaucomatous feature sets. A total of 40 samples, 20 glaucomatous and 20 non-glaucomatous are used to train the BPNN.

**CHAPTER 4**

**TESTING, RESULTS AND DISCUSSION**

## 4.1 Extraction and Measuring the Cup to Disc Ratio

A total of 166 images were examined by the department of optometry and visual science in KNUST. The images below are samples of the automatic extraction of the OC and OD verses the manual markings of OC and OD by the eye specialists.



(a)  (b)  (c)

(d)  (e)  (f)
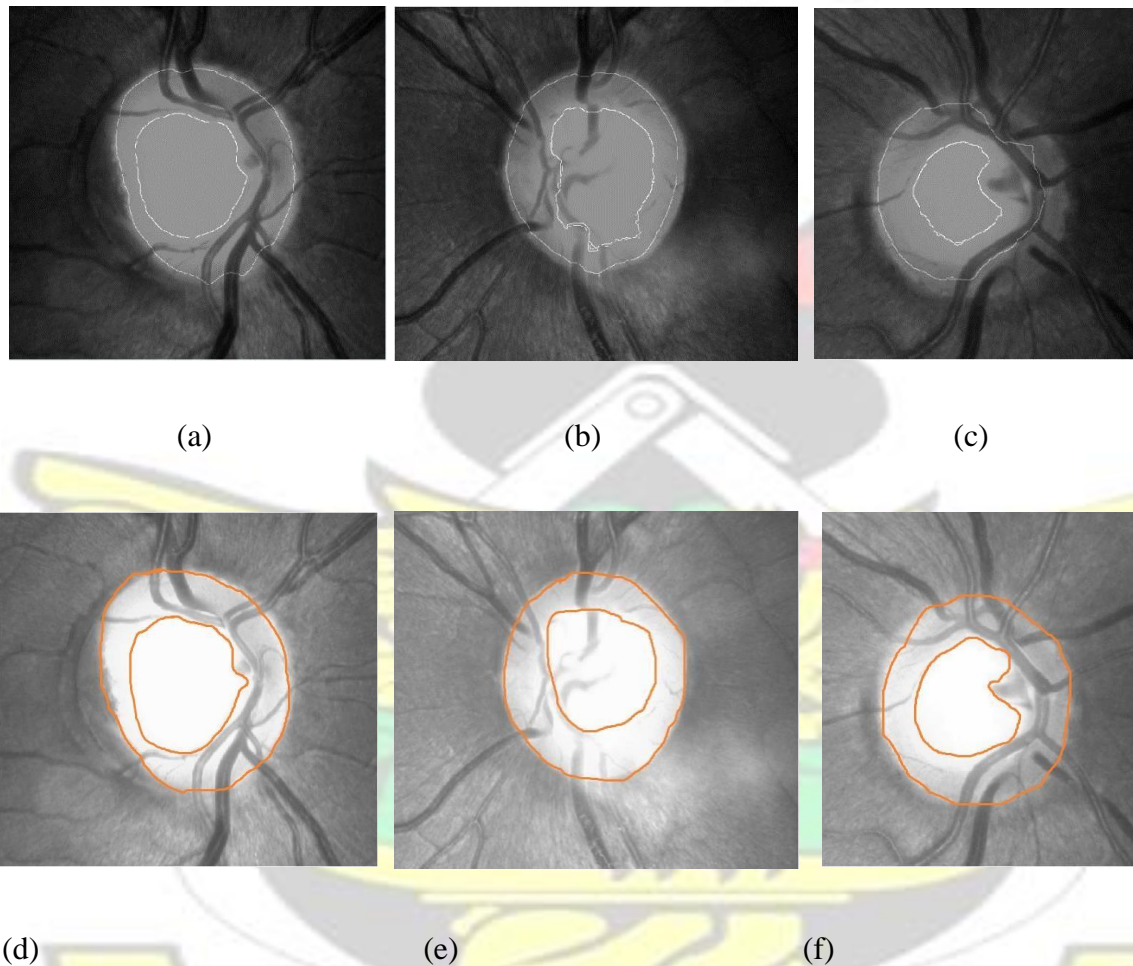
**Figure 4.1 Manual verses automatic OD and OC extraction**

Apart from the 40 images used to train the system, 126 were then used to assess the algorithm. The graph below shows values of the vCDR as measured by the algorithm verses that measured by the eye specialists for 126 fundus images-
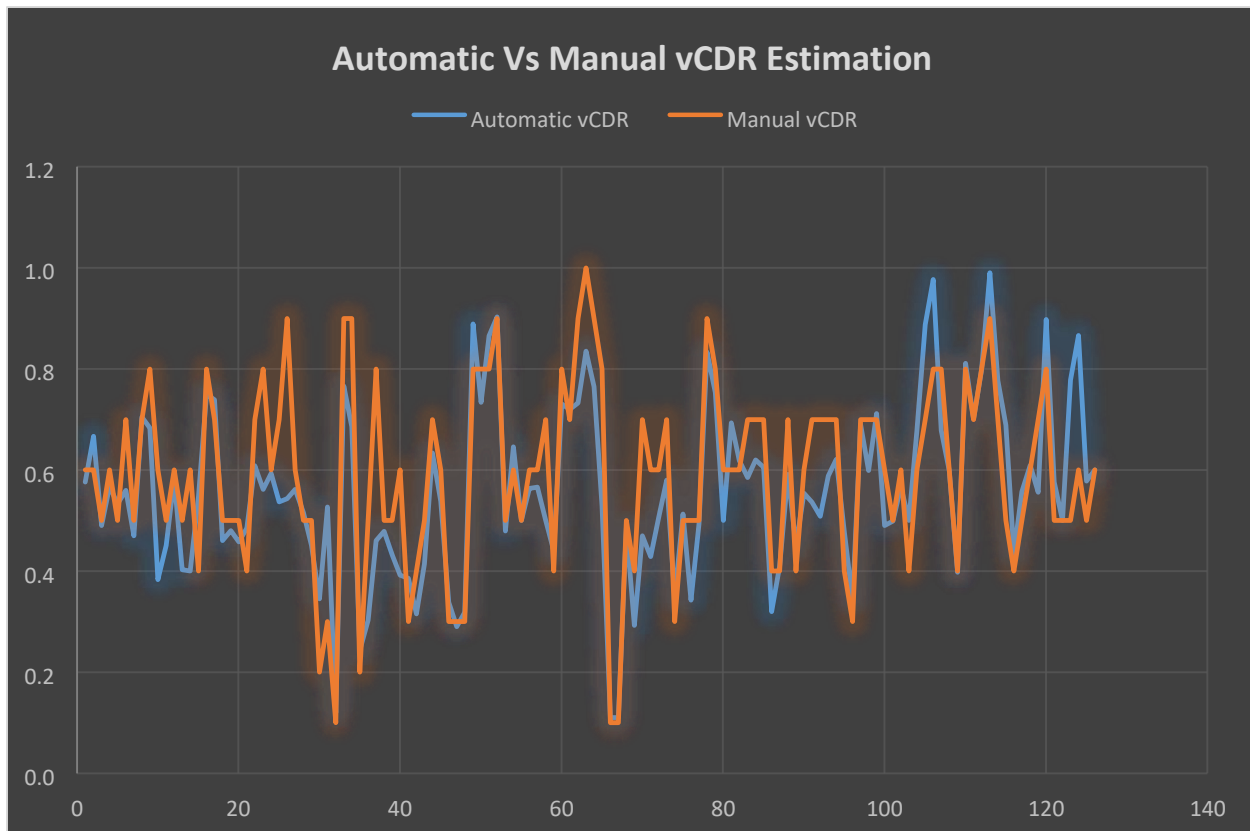
**Figure 4.2 Automatic Verses Manual CDR Estimation**

From the graph, it appears that the automatic system has a tendency to underestimate the vCDR. To present a more objective assessment, we performed a T-test on the two datasets, to find if the mean of the two datasets were significantly different, thus if the estimated values were essentially the same. The null hypothesis is that there is no difference greater than 0.05 between the values estimated by the algorithm, and the values given by the trained eye specialists. Usually, a tolerance of +/- 0.1 is acceptable even amongst eye specialists. To make our test more stringent, we chose a difference of 0.05. The t-test returned a probability of 2.08E-13% chance that the datasets were different. This is far greater than the typical 5% threshold based on which the null hypothesis could be rejected. With a probability of 2.08E-13%, the null hypothesis is not rejected. We also found the root mean square error (RMSE) of the automatic segmentation as against that of the eye

specialists. The RMSE is calculated as the square root of the variance of the differences (*residuals)* between the observed value and the value predicted by the algorithm.

The RMSE is generally a good measure of the accuracy of a system at predicting a correct response. The lower the RMSE, the more accurate the system. The proposed algorithm achieved an RMSE of 0.11.

**TABLE 4.1 PERFORMANCE OF PROPOSED ALGORITHM WITH ANOTHER ALGORITHM FOR vCDR ESTIMATION**

| Method | Error Assessment | Measurement Error Rates |
|---|---|---|
| Proposed Method | Root Mean Square Error | 0.11 |
| AGLAIA [39] | Root Mean Square Error | 0.26 |

In the pre-processing block, the blurriness metric ensures that the right threshold value is selected for subsequent threshold. Even though PCNN adequately prepares the images for thresholding, for images that are blur (usually from the capturing device), it was observed that the thresholding was usually not correct, before the introduction of the blurriness measurement step. The optic cup was underestimated in such cases, and the extraction of cup and disc was wrong. Thus, the blurriness detection step greatly enhanced the performance of the system.

The blood vessels removal step also proves very useful, as the entire algorithm relies on the variation of pixel intensity values of the optic cup and the optic disc. The presence of blood vessels on the image serve as noise.

For CADx application, the algorithm presents the eye specialist with the opportunity to measure and obtain objective assessments of the ratio of the optic cup and disc from many angles on the

image. For use by patients unaided by an eye specialist, the algorithm selects the typical best vertical line to measure the vCDR and ISNT rule.



(a)                                      (b)                                      (c)
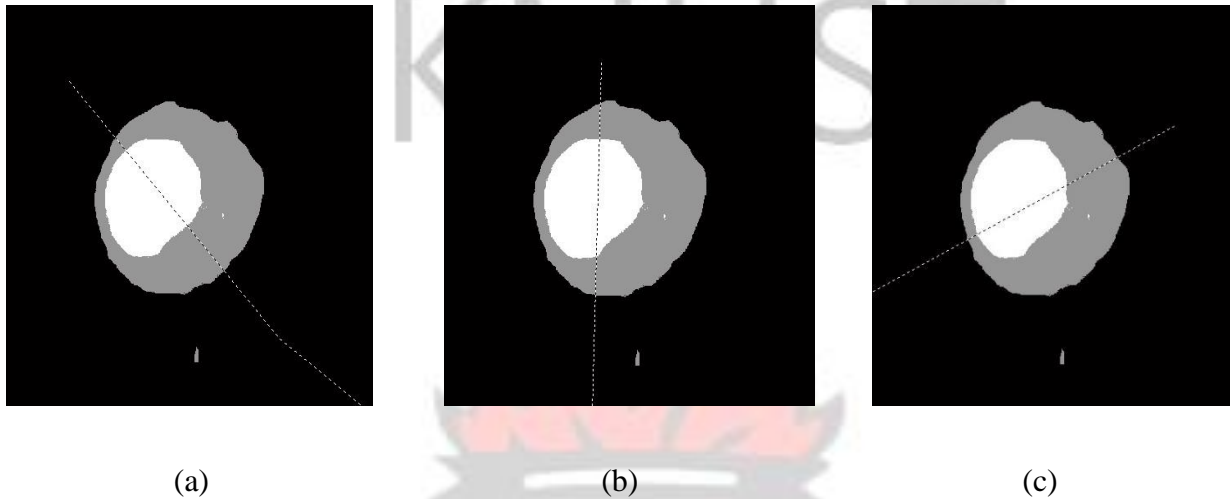
**Figure 4.3 – vertical lines assessing vCDR manually drawn by eye specialist**

**4.3 Predicting Glaucoma**

The entire essence of measuring the vCDR and ISNT rule is to be able to predict Glaucoma. According to the department of optometry and visual science, a vCDR less than 0.4 is indicative of a normal cup. A vCDR of above 0.5 requires the evaluation of the ISNT rule to confirm suspicion of glaucoma.

A total of 44 images were marked as suspicious for glaucoma by the eye specialists. The remaining 82 were classified as normal. The system was able to correctly classify 39 images as suspicious. 7 images were wrongly classified as suspicious. A total of 82 images were normal, and the system correctly classified 75 out of that. 5 images were wrongly classified as normal. The table below gives a summary

**TABLE 4.2 RESULTS**

| Automated Prediction Glaucoma | Positive Test Outcome | True Positive (TP) = 39 | False Positive (FP) = 7 | Positive Predictive Value =TP/(TP + FP) =39/(39+7) = 84.7% |
|---|---|---|---|---|
| | Negative Test Outcome | False Negative (FN) = 5 | True Negative (TN) = 75 | Negative Predictive Value = TN/ (FN + TN) = 75/ (5 + 75 ) = 93.75% |
| | | Sensitivity = TP / (TP + FN ) = 39 / ( 39 + 5 ) = 88.6% | Specificity = TN / ( FP + TN ) = 75 / ( 7 + 75 ) = 91.4% | |

## 4.4 Discussion

The line profile approach has the advantage of eliminating the contribution of noise in estimating the vCDR. In the method proposed by [27] for example, the CDR is estimated by counting white pixels after thresholding and segmenting cup and disc. For imperfect segmentation of cup and disc, there is an overestimation of cup size due to the presence of other white pixels in the image (noise). The line profile approach makes it possible to avoid these errors, and provide a more accurate estimation of cup and disc ratio. Figure 4.3 illustrates this with a typical fundus image that contains some noise introduced during the capture stage of the image.
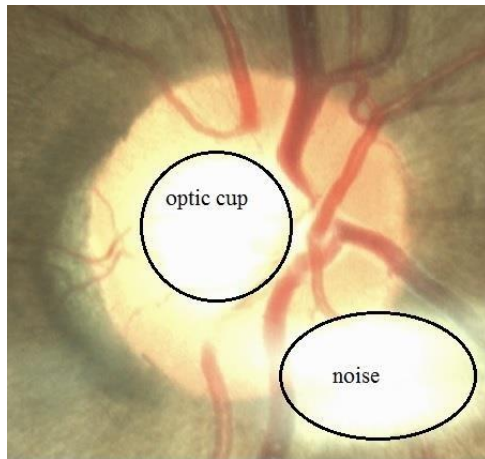
(a)
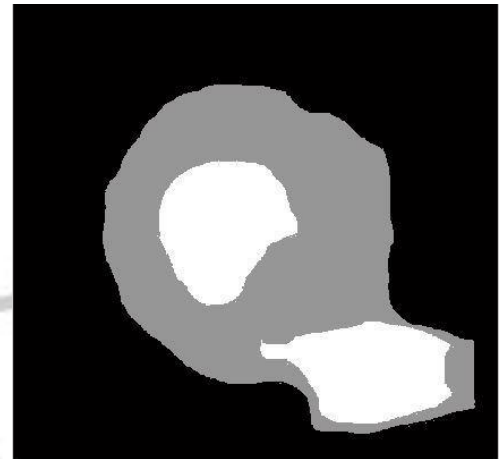


(b)
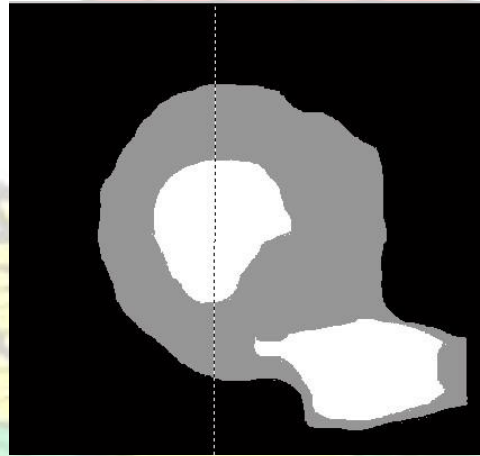


(c)

**Figure 4.4 Line profile algorithm and noise (a – original image showing noise, b – segmented image with noise, c- line profile eliminates the effect of noisy pixels)**

The ability of the system to correctly identify suspicious glaucomatous discs is referred to as the sensitivity of the system. Our system achieved a sensitivity of 88.6%. The system achieved a low number of false positives and few false negatives showing that a positive screen test is reliable in itself at confirming that a patient may have a glaucomatous disc. The system achieved a high Positive Predictive Value of 84.7%.

An advantage of the system is the high Negative Prediction Value (NPV). This is desirable for a screening system, as it is reassuring to a patient to know that he is most likely not to have glaucoma. The NPV was 93.75%. The ability of the system to correctly classify patients as not likely to have glaucoma is known as the specificity. Our system achieved a specificity of 91.4%.

For an objective assessment of our system, we compared the balanced accuracy of our system to that of other systems in literature. The balanced accuracy accounts for the differences in data size, and presents an objective assessment of the performance of the system [40]. The balanced accuracy is calculated as $\frac{sensitivity+specificity}{2}$. The table below shows the performance of our proposed algorithm with other algorithms –

TABLE **4.3** COMPARISON OF PROPOSED METHOD WITH OTHER METHODS

| Method | Number of Images | Specificity | Sensitivity | Balanced Accuracy |
|--------|------------------|-------------|-------------|-------------------|
| Agarwal et al [41] | 60 | 80% | 100 % | 90% |
| Hatanaka et al [26] | 79 | 85% | 80% | 82.5% |
| Hana et al [42] | 60 | 88% | 92.3% | 90.15% |
| Proposed Method | 126 | 91.4% | 88.6% | 90% |

**4.5 Findings**

A total of 9 images that were classified as suspicious for glaucoma by the system, was another ocular malady known as optic nerve atrophy. The department of Optometry classified the image as suspicious as well, but indicated it was optic nerve atrophy. Optic nerve atrophy could have varied causes including glaucoma. Thus an atrophied disc may not necessarily imply glaucoma.

The system is thus able to detect at least another ocular malady apart from its main goal, which is glaucoma prediction. This may indicate that the system is useful for evaluating eye diseases that affect the optic nerve in general, and cause morphological changes to the optic cup and disc.

**CHAPTER 5**

# CONCLUSION AND RECOMMENDATIONS

## 5.1 Conclusion

In conclusion, a new image processing algorithm was proposed to extract vital clinical features from fundus images for the prediction of Glaucoma in Ghana. Even though diagnosis of glaucoma is based on several variables, the vCDR, and ISNT rule evaluation is traditionally the first parameters to assess clinically when imaging modalities are used. The proposed algorithm improves on the work of [26], by innovatively extracting the critical diagnostic features for the classifier. Our algorithm uses PCNN to preprocess the image, in order to remove noisy pixels and ensure that the thresholding stage is effective. In the event of noisy pixels present in the finally segmented image, the line profile approach is able to accurately estimate the vCDR without being affected by the noisy pixels.

The proposed method has a specificity of 91.4% with a sensitivity of 88.6%. This makes the system reliable. The method of analyzing the extracted features to compute the vCDR is also novel, and proves to be very effective.

Again, the introduction of the PCNN processing stage before thresholding ensures a bi-modal histogram of the image, separating the background from the OD area. This challenge in the development of image processing algorithms based on thresholding is thus mitigated with the use of a PCNN before the thresholding is attempted.

## 5.2 Future Work

The section shows future work associated with this research. In order to increase the sensitivity, a neural network that uses radial functions as activation functions for the subsequent classification of extracted features as that would give a more accurate prediction.

Radial functions are generally more accurate than BPNNs, and perform multi-class classification. This can extend the system to identify different stages of glaucoma.

Again, further research can go into combining images from another imaging modality preferably Optical Coherence Tomography (OCT) machines and Fundus images for prediction of glaucoma, Further research will also go into the possibility of employing the proposed algorithm for automatic tumor detection and measurement in order to enhance CADx for other medical images, e.g. brain scans

## References

[1] "Glaucoma Facts and Statistics," 5 April 2011. [Online]. Available:
http://www.glaucoma.org/glaucoma/facts-statistics/glaucoma-facts-and-stats.php.
[Accessed 26 May 2015].

[2] Michael E. Gyasi, A.W. Francis, Y. Chen, R.S.R Harrison, A.R Kodjo, "Presentation of Glaucoma in the Greater Accra Metropolitan Area of Ghana," *Ghana Medical Journal,* vol. 48, no. Number 3, pp. 143-147, 2014.

[3] Michael E Gyasi, "Comparison of Primary Open Angle Glaucoma Patients in Rural and Urban Ghana," vol. 14, no. 3, pp. 729-735, 2014.

[4] Ghana Statistical Service, "2010 Population and Housing Census - Summary of report of final results," Ghana Statistical Servce, Accra, May, 2010.

[5] Japan Glaucoma Society, Guidelines for Glaucoma (2nd Edition), 4F, Hongo hirano Bldg., 3-20-6 Hongo, Bunkyo-ku, Tokyo 113-0033 Japan: Japan Glaucoma Society, September 2006.

[6] National Health and Medical Research Center, Australian Government, NHMRC GUIDELINES FOR THE SCREENING, PROGNOSIS, DIAGNOSIS, MANAGEMENT AND PREVENTION OF GLAUCOMA, 2010.

[7] Citi Fm, "Ghana Has 26.09 million mobile phone users," 22 March 2013. [Online]. Available: http://www.ghanaweb.com/GhanaHomePage/NewsArchive/Ghana-has-26-09million-mobile-phone-users-268640. [Accessed 16 February 2016].

[8] D. Ljubimova, "Biomechanics of the Human Eye and Intraocular Pressure Measurements," Universitetservice US-AB, Royal Institute of Technology, Department of Mechanics - SE100 44, Stockholm, Sweden, 2009.

[9] J Crawford Downs, Michael D Roberts, Claude F Burgoyne, "The Mechanical Environment of the Optic Nerve Head In Glaucoma," PMC, 23 July 2009. [Online]. Available: http://www.ncbi.nlm.nih.gov/pmc/articles/PMC2714589/. [Accessed 16 March 2016].

[10] Simmmons, C Ross Ethier and Craig A, Introductory Biomechanics From Cells to Organisms, New York: Cambridge University Press, 2007.

[11] Guyton Arthur C,, Textbook of medical physiology / Arthur C. Guyton, John E. Hall.— 11th ed., Elsavier ISBN 0-7216-0240-1.

[12] Gardiner BS, Smith DW, Coote M, Crowston JG, "Computational Modeling of Fluid Flow and Intra-Ocular Pressure following Glaucoma Surgery," *Plus ONE,* vol. 5(10), no. e13178,, p. doi:10.1371/journal.pone.0013178, 2010.

[13] A. B. Bruce James, Ophthalmology, Lecture Notes 11th Edition, United Kingdom: John Wiley & Sons, Inc, Publications, 2011.

[14] D. L. Budenz, "Global Perspectives on African Glaucoma," Accra, 2010, 6 August.

[15] Zhuo Zhang, Ruchir Srivastava, Huiying Liu, Xiangyu Chen, Lixin Duan, Damon Wing kee Wong, Chee Keong kwoh, Tien Yin Wong, Jiang Liu, "A survey on computer aided diagnosis for ocular diseases," no. Zhang et al. BMC Medical Informatics and Decision Making 2014, 14:80, 2014.

[16] Matsui M, Tashiro T, Matsumoto K, Yamamoto S, "A study on automatic and Quantitative diagnosis of fundus photographs. I. detection of contour line of retinal blood vessel images on color fundus photographs," vol. 77(8):907, 1973.

[17] Baudoin C, Lay B, Klein J, "Automatic detection of microaneurysms in diabetic fluorescein angiography," Vols. 32(3-4):254, 1984.

[18] Antal B, Hajdu A, "An ensemble-based system for microaneurysm detection and diabetic retinopathy grading," vol. Trans Biomed Eng, no. 59(6):1720-1726, 2012.

[19] Harangi B, Lazar I, Hajdu A, "Automatic Exudate Detection using active contour model and regionwise Classification," vol. IEEE; 2012, no. :5951-4, 2012.

[20] Martins CIO, Medeiros F, Veras RM, Bezerra FN, Cesar R, "Evaluation of Retinal Vessel Segmentation Methods for Microaneurysms Detection," 2009.

[21] Jaafar HF, Nandi AK, Al-Nuaimy W, "Detection of Exudates in Retinal Images Using A Pure Splitting Technique," 2010.

[22] Walter T, Massin P, Erginay A, Ordonez R, Jeulin C, Klein JC, "Automatic Detection of Microaneurysms in Color Fundus Images.," Vols. 11(6):555-556, 2007.

[23] H. A. Lazar I, "Retinal Microaneurysm Detection through Local Rotating Cross-Sectional Profile Analysis," no. 32(2):400-407, 2013.

[24] Fleming AD, Philip S, Goatman KA, Olson JA, Sharp PF, "Automated microaneurysm Detection Using Local Contrast Normalization and Local Vessel Detection," vol. 25(9), no. 1223-1232, 2006.

[25] Esmaeili M, Rabbani H, Dehnavi AM, Dehghani A, "A new Curvelet transform Based method for extraction of red lesions in digital color retinal Images," 2010.

[26] Yuji Hatanaka, Atsushi Noudo, Chisako Muramatsu, Akira Sawada, Takeshi Hara, Tetsuya Yamamoto, Hiroshi Fujita, "Vertical cup-to-disc ratio measurement for diagnosis of glaucoma on fundus images," Vols. 7624, 76243C, 2010.

[27] S. T. Kumika Choudhary, "ANN Glaucoma Detection Using Cup-to-Disk Ratio and Neuroretinal Rim," vol. 111, no. 11, 2015.

[28] J. A. M. Mario I. Chacon, "A PCNN-FCM time series classifier for texture segmentation," Vols. Fuzzy Information Processing Society (NAFIPS), 2011 Annual Meeting of the North American, no. 11962070, 2011.

[29] Juan A. Ramirez-Quintana, Mario I. Chacon-Marguia and Jose F. Chacon-Hinojos, "Artificial Nerual Image Processing Applications: A Survey," vol. 20:1, 2012.

[30] Zhaobin Wang, Yide Ma, Feiyan Cheng and Lizhen Yang, "Review Of Pulse-coupled neural network," Vols. 28(2010)5-13, 2010.

[31] Vinícius Gonçalves Maltarollo, Káthia Maria Honório and Albérico Borges Ferreira da Silva, "Applications of Artificial Neural Networks in Chemical Problems," in *Artificial Neural Networks - Architectures and Applications*, ISBN: 978-953-51-0935-8, InTech, DOI: 10.5772/51275, 2013.

[32] E. Alpaydin, Introduction to Machine Learning, Cambridge, Massachusetts, London, England: The MIT Press, 2004.

[33] McCulloch, W. S., & Pitts W., "A logical Calculus of the Ideas Imminent in nervous activity," Vols. 5, 115-133, 1943.

[34] Reinhard Eckhorn, Herbert J Reitboeck, Martin Ardnt and Peter Dicke, "Feature Linking Via Stimulus - Evoked Oscillations: Experimental results from Cat visual Cortex and Functional Implications from a network Model," Vols. Neural networks, 1989. IJCNN, International Joint Conference On, no. 723-730 Vol 1, 1989.

[35] M. Cilimkovic, "Neural Networks and Back Propagation Algorithm," Institute of Technology Blanchardstown, Dublin 15, Ireland.

[36] Robl N Maamari, Jeremy D Keenan, Daniel A Fletcher, Todd P Margolls, "A Mobile Phone-based Retinal Camera for Portable Wide Field Imaging," no. Br J Ophthalmol. 2014;98(4):438441, 2012.

[37] F Dolmiere T., Ladret P., Nicolas M Grenoble, "The Blur Effect : Perception and Estimation with a New No-Reference Perceptual Blur Metric," *SPIE Electronic Imaging Symposium Conf human Vision and Electronic Imaging, Etats-Unis D'Amerique,* 2007.

[38] Qu Xiao-Bo, Yan Jing-Wen, Xiao Hong-Zhi, Zhu Zi-Qian, "Image Fusion Algorithm based on Spatial Frequency Motivated Pulse Coupled Neural Networks In Nonsubsampled Contourlet Transform Domain," *Acta Automatica Sinica,* Vols. 34,, no. 12,, pp. pp: 15081514, Dec, 2008.

[39] J. Liu, F.S Yin, D.W.K Wong, Z, Zhang, N.M Tan, C.Y Cheug, M. Baskaran, T. Aung and T.Y Wong, "Automatic Glaucoma Diagnosis from Fundus Image," *33rd Annual International Conference of the IEEE EMBS,* Vols. Boston, Massachusetts USA, August 20 - September 3,, 2011.

[40] Kay H. Brodersen, Cheng Soon Ong, Klaas E. Stephen and Joachim M Buhman, "The Balanced Accuracy and its posterior distribution," in *International Conference on Pattern Recognition*, 2010.

[41] Ayushi Agarwal, Shradha Gulia, Somal Chaudhary, Carlos M. Travieso, Jesus B. AlonsoHernandez, "A Novel Approach to Detect Glaucoma in Retinal Fundus Images using CupDisk and Rim-Disk Ratio," *IEEE,* no. 978-1-4673-7846-8/15/$31.00 ©2015 IEEE, 2015.

[42] Hanan Alghmdi, Hongying Lilian Tang, Morten Hansen, Arrianne O'Shea, Lutfiah Al turk, Tunde Peto, "Measurement of Optical Cup-to-disc ratio in Fundus Images for Glaucoma screening," in *IEEE*, 2015.

# APPENDIX A – vCDR ESTIMATION DATA

| | Automatic | | Squared Image | vCDR | Manual vCDR | Residuals |
|---|---|---|---|---|---|---|
| | Residuals | | | | | |
| 1 | 0.5763 | 0.6 | 0.0237 | 0.00056169 | | |
| 2 | 0.6667 | 0.6 | -0.0667 | 0.00444889 | | |
| 3 | 0.4902 | 0.5 | 0.0098 | 9.604E-05 | | |
| 4 | 0.5676 | 0.6 | 0.0324 | 0.00104976 | | |
| 5 | 0.5333 | 0.5 | -0.0333 | 0.00110889 | | |
| 6 | 0.56 | 0.7 | 0.14 | 0.0196 | | |
| 7 | 0.4697 | 0.5 | 0.0303 | 0.00091809 | | |
| 8 | 0.7049 | 0.7 | -0.0049 | 2.401E-05 | | |
| 9 | 0.6833 | 0.8 | 0.1167 | 0.01361889 | | |
| 10 | 0.3833 | 0.6 | 0.2167 | 0.04695889 | | |
| 11 | 0.451 | 0.5 | 0.049 | 0.002401 | | |
| 12 | 0.5833 | 0.6 | 0.0167 | 0.00027889 | | |
| 13 | 0.4028 | 0.5 | 0.0972 | 0.00944784 | | |
| 14 | 0.4 0.6 | 0.2 | 0.04 | | | |
| 15 | 0.5484 | 0.4 | -0.1484 | 0.02202256 | | |
| 16 | 0.75 | 0.8 | 0.05 | 0.0025 | | |
| 17 | 0.7391 | 0.7 | -0.0391 | 0.00152881 | | |
| 18 | 0.4603 | 0.5 | 0.0397 | 0.00157609 | | |
| 19 | 0.48 | 0.5 | 0.02 | 0.0004 | | |
| 20 | 0.4578 | 0.5 | 0.0422 | 0.00178084 | | |
| 21 | 0.4848 | 0.4 | -0.0848 | 0.00719104 | | |
| 22 | 0.6087 | 0.7 | 0.0913 | 0.00833569 | | |
| 23 | 0.5616 | 0.8 | 0.2384 | 0.05683456 | | |
| 24 | 0.5932 | 0.6 | 0.0068 | 4.624E-05 | | |
| 25 | 0.5373 | 0.7 | 0.1627 | 0.02647129 | | |
| 26 | 0.5432 | 0.9 | 0.3568 | 0.12730624 | | |
| 27 | 0.5616 | 0.6 | 0.0384 | 0.00147456 | | |
| 28 | 0.5152 | 0.5 | -0.0152 | 0.00023104 | | |
| 29 | 0.4507 | 0.5 | 0.0493 | 0.00243049 | | |
| 30 | 0.3452 | 0.2 | -0.1452 | 0.02108304 | | |
| 31 | 0.527 | 0.3 | -0.227 | 0.051529 | | |
| 32 | 0.12 | 0.1 | -0.02 | 0.0004 | | |
| 33 | 0.7662 | 0.9 | 0.1338 | 0.01790244 | | |
| 34 | 0.686 | 0.9 | 0.214 | 0.045796 | | |
| 35 | 0.2432 | 0.2 | -0.0432 | 0.00186624 | | |
| 36 | 0.3026 | 0.5 | 0.1974 | 0.03896676 | | |
| 37 | 0.4605 | 0.8 | 0.3395 | 0.11526025 | | |

| | | | | |
|---|---|---|---|---|
| 38 | 0.4789 | 0.5 | 0.0211 | 0.00044521 |
| 39 | 0.4324 | 0.5 | 0.0676 | 0.00456976 |
| 40 | 0.3919 | 0.6 | 0.2081 | 0.04330561 |
| 41 | 0.3857 | 0.3 | -0.0857 | 0.00734449 |
| 42 | 0.3151 | 0.4 | 0.0849 | 0.00720801 |
| 43 | 0.4143 | 0.5 | 0.0857 | 0.00734449 |
| 44 | 0.6338 | 0.7 | 0.0662 | 0.00438244 |
| 45 | 0.5385 | 0.6 | 0.0615 | 0.00378225 |
| 46 | 0.3382 | 0.3 | -0.0382 | 0.00145924 |
| 47 | 0.2903 | 0.3 | 0.0097 | 9.409E-05 |
| 48 | 0.3188 | 0.3 | -0.0188 | 0.00035344 |
| 49 | 0.8889 | 0.8 | -0.0889 | 0.00790321 |
| 50 | 0.7342 | 0.8 | 0.0658 | 0.00432964 |
| 51 | 0.8657 | 0.8 | -0.0657 | 0.00431649 |
| 52 | 0.9028 | 0.9 | -0.0028 | 7.84E-06 |
| 53 | 0.4795 | 0.5 | 0.0205 | 0.00042025 |
| 54 | 0.6456 | 0.6 | -0.0456 | 0.00207936 |
| 55 | 0.5 | 0.5 | 0 | 0 |
| 56 | 0.5634 | 0.6 | 0.0366 | 0.00133956 |
| 57 | 0.5663 | 0.6 | 0.0337 | 0.00113569 |
| 58 | 0.5 | 0.7 | 0.2 | 0.04 |
| 59 | 0.44 | 0.4 | -0.04 | 0.0016 |
| 60 | 0.7308 | 0.8 | 0.0692 | 0.00478864 |
| 61 | 0.72 | 0.7 | -0.02 | 0.0004 |
| 62 | 0.7324 | 0.9 | 0.1676 | 0.02808976 |
| 63 | 0.8354 | 1 | 0.1646 | 0.02709316 |
| 64 | 0.7647 | 0.9 | 0.1353 | 0.01830609 |
| 65 | 0.5286 | 0.8 | 0.2714 | 0.07365796 |
| 66 | 0.11 | 0.1 | -0.01 | 1E-04 |
| 67 | 0.11 | 0.1 | -0.01 | 1E-04 |
| 68 | 0.4857 | 0.5 | 0.0143 | 0.00020449 |
| 69 | 0.2927 | 0.4 | 0.1073 | 0.01151329 |
| 70 | 0.4699 | 0.7 | 0.2301 | 0.05294601 |
| 71 | 0.4286 | 0.6 | 0.1714 | 0.02937796 |
| 72 | 0.506 | 0.6 | 0.094 | 0.008836 |
| 73 | 0.5802 | 0.7 | 0.1198 | 0.01435204 |
| 74 | 0.3488 | 0.3 | -0.0488 | 0.00238144 |
| 75 | 0.5132 | 0.5 | -0.0132 | 0.00017424 |
| 76 | 0.3425 | 0.5 | 0.1575 | 0.02480625 |
| 77 | 0.4932 | 0.5 | 0.0068 | 4.624E-05 |
| 78 | 0.8333 | 0.9 | 0.0667 | 0.00444889 |

| | | | | |
|---|---|---|---|---|
| 79 | 0.7536 | 0.8 | 0.0464 | 0.00215296 |
| 80 | 0.5 | 0.6 | 0.1 | 0.01 |
| 81 | 0.6933 | 0.6 | -0.0933 | 0.00870489 |
| 82 | 0.6184 | 0.6 | -0.0184 | 0.00033856 |
| 83 | 0.5854 | 0.7 | 0.1146 | 0.01313316 |
| 84 | 0.6197 | 0.7 | 0.0803 | 0.00644809 |
| 85 | 0.6056 | 0.7 | 0.0944 | 0.00891136 |
| 86 | 0.32 | 0.4 | 0.08 | 0.0064 |
| 87 | 0.41 | 0.4 | -0.01 | 1E-04 |
| 88 | 0.5915 | 0.7 | 0.1085 | 0.01177225 |
| 89 | 0.45 | 0.4 | -0.05 | 0.0025 |
| 90 | 0.5541 | 0.6 | 0.0459 | 0.00210681 |
| 91 | 0.5362 | 0.7 | 0.1638 | 0.02683044 |
| 92 | 0.5088 | 0.7 | 0.1912 | 0.03655744 |
| 93 | 0.5882 | 0.7 | 0.1118 | 0.01249924 |
| 94 | 0.6212 | 0.7 | 0.0788 | 0.00620944 |
| 95 | 0.4789 | 0.4 | -0.0789 | 0.00622521 |
| 96 | 0.3425 | 0.3 | -0.0425 | 0.00180625 |
| 97 | 0.69 | 0.7 | 0.01 | 0.0001 |
| 98 | 0.599 | 0.7 | 0.101 | 0.010201 |
| 99 | 0.712 | 0.7 | -0.012 | 0.000144 |
| 100 | 0.49 | 0.6 | 0.11 | 0.0121 |
| 101 | 0.499 | 0.5 | 0.001 | 0.000001 |
| 102 | 0.567 | 0.6 | 0.033 | 0.001089 |
| 103 | 0.5 | 0.4 | -0.1 | 0.01 |
| 104 | 0.678 | 0.6 | -0.078 | 0.006084 |
| 105 | 0.888 | 0.7 | -0.188 | 0.035344 |
| 106 | 0.977 | 0.8 | -0.177 | 0.031329 |
| 107 | 0.678 | 0.8 | 0.122 | 0.014884 |
| 108 | 0.599 | 0.6 | 0.001 | 0.000001 |
| 109 | 0.398 | 0.4 | 0.002 | 4E-06 |
| 110 | 0.811 | 0.8 | -0.011 | 0.000121 |
| 111 | 0.701 | 0.7 | -0.001 | 0.000001 |
| 112 | 0.798 | 0.8 | 0.002 | 4E-06 |
| 113 | 0.99 | 0.9 | -0.09 | 0.0081 |
| 114 | 0.777 | 0.7 | -0.077 | 0.005929 |
| 115 | 0.689 | 0.5 | -0.189 | 0.035721 |
| 116 | 0.435 | 0.4 | -0.035 | 0.001225 |
| 117 | 0.557 | 0.5 | -0.057 | 0.003249 |

| 118 | 0.609 | 0.6 | -0.009 | 8.1E-05 |
|---|---|---|---|---|
| 119 | 0.556 | 0.7 | 0.144 | 0.020736 |
| 120 | 0.898 | 0.8 | -0.098 | 0.009604 |
| 121 | 0.576 | 0.5 | -0.076 | 0.005776 |
| 122 | 0.5 | 0.5 | 0 | 0 |
| 123 | 0.778 | 0.5 | -0.278 | 0.077284 |
| 124 | 0.866 | 0.6 | -0.266 | 0.070756 |
| 125 | 0.578 | 0.5 | -0.078 | 0.006084 |
| 126 | 0.6001 | 0.6 | -1E-04 | 1E-08 |

## APP\ENDIX B -MATLAB CODE

```
%% RESET & INITIALIZE
%tic clc
clear all
close all
warning off %#ok<WNOFF> set(0,'DefaultFigureWindowStyle','docked')
%% LOADING IMAGE %%%
[x,storedColorMap]=imread('Image76.jpg');
togglefig('Original Image') h(1)=imshow(x);


%% Morphological Operation On ROI
tic
Strel=strel('disk',20); outb=imclose(x,Strel);
togglefig('Morphologically Operated On')
imshow(outb); x=outb; toc %% tic
[r,g,b,H,h,s,v]=Split(x);
[countb,Graylevelb]=imhist(b);
maxGLValueb=find(countb > 0, 1, 'last');
maxcountb=max(countb); figure,
bar(countb,'b'); toc %%%% tic
figure, imshow(b);
f=fspecial('gaussian',[12 12],0.9);
t=imfilter(b,f); figure, imshow(t)
toc %% PCNN imblue=double(t); tic
link_arrange=8;
iteration_times=20;
firing_times=PCNN_large_arrange(imblue,link_arrange,iteration_times);
% figure,imshow(imblue,[])
figure,imshow(firing_times,[])




toc %% PCNN Image I =
firing_times; b = dec2bin(I); % b
becomes vector % some actions
with binary vector du =
bin2dec(b);
```

```
du = reshape(du,size(I)); % converting vector du to 3d Image array
du=du.*10.0; imwrite(uint8(du), 'du.jpg'); %save our du to file
du.jpg

I = imread('du.jpg'); %test if it saved correctly figure,imshow(I)

%% tic
[threshb,metricb]=multithresh(I,2);
toc %%
bluethresholdlow=max(threshb); bluethresholdhigh=255;
bluemask=(I>=bluethresholdlow) & (I<=bluethresholdhigh); figure,
imshow(bluemask)
%%
edgeB=edge(bluemask,'canny',0.4); figure,
imshow(edgeB)
%%
[countR,GraylevelR]=imhist(r);
maxGLValueR=find(countR > 0, 1, 'last');
maxcountR=max(countR); figure,
bar(countR,'r');
%%
Strel=strel('disk',18);
outr=imclose(r,Strel);
figure, imshow(outr);
r=outr; %% %PCNN
imred=double(r); tic
link_arrange=8;
iteration_times=20;
firing_times=PCNN_large_arrange(imred,link_arrange,iteration_times);
% figure,imshow(imred,[])
figure,imshow(firing_times,[])
toc
%PCNN Image
I = firing_times;
R = dec2bin(I); % b becomes vector %
some actions with binary vector du =
bin2dec(R);
du = reshape(du,size(I)); % converting vector du to 3d Image array  du=du.*10.0;
imwrite(uint8(du), 'du.jpg'); %save our du to file du.jpg
I = imread('du.jpg'); %test if it saved correctly
```

```matlab
imshow(I)

%% [threshr,metricr]=multithresh(I,2);
%%
redthresholdlow=max(threshr); redthresholdhigh=255;
redmask=(I>=redthresholdlow) & (I<=redthresholdhigh);
figure, imshow(redmask,[])
%%
edgeR=edge(redmask,'canny',0.4); figure,
imshow(edgeR)
%%
test2=imfuse(redmask,bluemask); figure,
imshow(test2)
   %%
test=imfuse(edgeB,edgeR); figure,
imshow(test)


%% CD
%cup=sum(bluemask(:));
%disc=sum(redmask);
%CDR=(cup/disc) %%
test2rgb=rgb2gray(test2); figure,
imshow(test2rgb);
   %%
c=improfile(100);
toc figure,
plot(c)
%%
[vCDR,IQ,SQ]=ISNTevaluation(c);
IS = IQ/SQ;    %%
imshow(test2rgb);
c=improfile(100);
toc
%figure, plot(c)
[vCDR,IQ,SQ]=ISNTevaluation(d);
NT = SQ/IQ;
%%
F=[vCDR,IS, NT]' toc

function R=PCNN_large_arrange(matrix,link_arrange,np,pre_flag)

disp('PCNN is processing...')
[p,q]=size(matrix);
% computes the normalized matrix of the matrixA and  matrixB
F_NA=Normalized(matrix);
alpha_L=1; alpha_Theta=0.2;
 beta=3; vL=1.00;
vTheta=20;
% Generate the null matrix that could be used
L=zeros(p,q);
```

```
U=zeros(p,q);
Y=zeros(p,q);
Y0=zeros(p,q);
Theta=zeros(p,q);
% Compute the linking strength.
center_x=round(link_arrange/2);
center_y=round(link_arrange/2);
W=zeros(link_arrange,link_arrange);
for i=1:link_arrange      for
j=1:link_arrange
        if (i==center_x)&&(j==center_y)
            W(i,j)=0;
else
            W(i,j)=1./sqrt((i-center_x).^2+(j-center_y).^2);
end      end end
%%%%%%%%%%%%%%%%%%%%%%%%%
F=F_NA; for n=1:np
    K=conv2(Y,W,'same');
    L=exp(-alpha_L)*L+vL*K;
    Theta=exp(-alpha_Theta)*Theta+vTheta*Y;
    U=F.*(1+beta*L);
    Y=im2double(U>Theta);
Y0=Y0+Y;      end R=Y0;
```